frontiers | Frontiers in Earth Science

TYPE Original Research
PUBLISHED 07 February 2025
DOI 10.3389/feart.2025.1545127

Check for updates

OPEN ACCESS

EDITED BY
Yong Wang,
Southwest Petroleum University, China

REVIEWED BY
Fangyang Hu,
Institute of Geology and Geophysics (CAS), China
Jing Guo,
Tianjin University of Commerce, China
Jiyong Li,
Southwest University of Science and Technology, China

*CORRESPONDENCE
Junaid Khan,
Junaidkhan5615@yahoo.com

RECEIVED 14 December 2024
ACCEPTED 14 January 2025
PUBLISHED 07 February 2025

CITATION
Lin Y, Yu C, Chen S, Shi S, Luo S and Khan J (2025) Paleozoic multi-stage magmatism in the Yuka terrane, North Qaidam orogenic belt: mantle modification, tectonic evolution, and geodynamic processes.
Front. Earth Sci. 13:1545127.
doi: 10.3389/feart.2025.1545127

COPYRIGHT
© 2025 Lin, Yu, Chen, Shi, Luo and Khan. This is an open-access article distributed under the terms of the Creative Commons Attribution License (CC BY). The use, distribution or reproduction in other forums is permitted, provided the original author(s) and the copyright owner(s) are credited and that the original publication in this journal is cited, in accordance with accepted academic practice. No use, distribution or reproduction is permitted which does not comply with these terms.

Paleozoic multi-stage magmatism in the Yuka terrane, North Qaidam orogenic belt: mantle modification, tectonic evolution, and geodynamic processes

Yibin Lin[1], Chengtao Yu[2], Shuyuan Chen[1], Sudong Shi[1], Sangjiancuo Luo[1] and Junaid Khan[3]*

[1]Tibet Xianglong Copper Industry Limited Company, Lhasa, Tibet, China, [2]Sixth Geological Brigade, Guangdong Geological Bureau, Guangdong, China, [3]School of Earth Resources, China University of Geosciences, Wuhan, China

The detailed study of HP/UHP metamorphic rocks and intermediate-acid rocks has revealed the complete tectonic evolution of the North Qaidam Orogenic Belt (NQOB), from oceanic to continental subduction and subsequent exhumation. However, less comprehensive studies of Paleozoic mafic rocks have led to a limited understanding of the subcontinental lithospheric mantle, geodynamic settings, and tectonic transitions. In this paper, a comprehensive study of mafic-intermediate rocks from the Yuka Terrane in the NQOB suggests that zircon U-Pb dating yielded ages of 471 ± 3 Ma and 438 ± 3 Ma, respectively. Both rocks exhibit arc-like trace element patterns, characterized by enrichment in REEs and LILEs (e.g., Cs, Rb, Ba, Th), depletion in HFSEs (e.g., Nb, Ta), moderate ($^{87}Sr/^{86}Sr$) i values (ranging from 0.70473 to 0.70811 and 0.70599 to 0.70685, respectively), and εNd(t) values ranging from positive to negative (−2.7 to +0.3 and −1.0 to +1.5, respectively), indicating derivation from the partial melting of enriched subcontinental lithospheric mantle. The current trace element compositions and previous studies on post-collisional mafic rocks suggest that the enriched material added to the subcontinental lithospheric mantle beneath the Qilian Block is primarily derived from fluids released by the subducting oceanic crust, with a smaller contribution from melts of overlying sediments. A comparison with previous studies, including mafic geochronological data and the period of UHP metamorphism, reveals that Paleozoic magmatism in the NQOB can be divided into three stages, while the NQOB experienced four distinct stages of geodynamic processes. These findings suggest a model of tectonic evolution and geodynamic transition: (1) 535–445 Ma: Slab retreat and associated back-arc extension; (2) 445–420 Ma: Slab rollback; (3) 420–395 Ma: Slab breakoff; (4) 395–360 Ma: Orogenic lithospheric collapse and extension. Overall, this study provides new insights into the nature of the subcontinental lithospheric mantle beneath the

Qilian Block, as well as the tectonic evolution and geodynamic processes within the NQOB.

KEYWORDS

multi-stage mafic magmatism, mantle modification, geodynamic processes, tectonic transition, North Qaidam

1 Introduction

The Collision orogenic belts may exhibit multi-stage mafic magmatism and ultrahigh-pressure (UHP) metamorphism, recording the evolutionary processes from oceanic subduction to continental subduction-collision, and eventually the post-collision phase. Mafic magmatism, in particular, is a response to geodynamic processes such as slab retreat and related back-arc extension, slab rollback, slab breakoff, as well as delamination and convective thinning of the lithosphere (Zhu et al., 2010; Wang et al., 2014; Song et al., 2015; Sun et al., 2018; Zhao et al., 2018; Fang et al., 2019; Gao et al., 2021; Niu et al., 2021; Zhou et al., 2021; Chen et al., 2024).

The geochemistry of mafic magma, often derived from ultramafic mantle sources, offers valuable insights into deep mantle processes and tectonic evolution (Hofmann, 1988; Chen et al., 2011; Wang et al., 2014; Cook et al., 2016; Zhao et al., 2018; Fang et al., 2019; Gao et al., 2021; Khan et al., 2023). For example, arc-like trace element compositions originating from the lithospheric mantle are modified by subducting crust (Zhao et al., 2013; Wu C. et al., 2014; Niu et al., 2021). During subduction, the oceanic or continental crust is pushed into the deep mantle, where metamorphic dehydration or partial melting forms fluids or melts from the slabs. These fluids or melts subsequently interact with the overlying mantle wedge, resulting in crust-mantle metasomatism at mantle depths (Roden and Murthy, 1985; Hofmann, 1997; Coltorti et al., 2007; Zheng, 2009; 2012; Zheng and Hermann, 2014; Fang et al., 2019; Niu et al., 2021; Chen et al., 2023; Guo et al., 2023).

Compared to subducting oceanic crust, the relatively low or dry geothermal gradient of continental subduction makes it more difficult for the subducting continental crust to release enough fluid to metasomatize the overlying mantle wedge (Hofmann, 1997; Herzberg, 2006; Chen and Zhao, 2017; Zheng and Chen, 2017; Fang et al., 2019; Chen et al., 2020; Niu et al., 2021), resulting in a general lack of arc volcanics coeval with continental subduction and the widespread presence of arc volcanics above oceanic subduction zones (Ernst and Liou, 1999; Rumble et al., 2003; Chung et al., 2005; Mo et al., 2008; Niu et al., 2013; McCarthy et al., 2018; Sun et al., 2018). Nevertheless, there are still small amounts of syn-collisional mafic magmatism in the continental margin above the subduction zone, such as the OIB-like mafic rocks found in the Sulu-Dabie orogen and the E-MORB-like or arc-like intermediate-mafic rocks found in the North Qaidam Orogenic Belt (NQOB) (Fang et al., 2019; Niu et al., 2021). The metasomatized mantle domains in orogenic belts serve as sources for syn-collisional mafic rocks. Additionally, some post-collisional mafic rocks originated from the mantle previously metasomatized by subduction-related fluids or melts, which is interpreted as delamination or convective thinning of the lithospheric mantle, leading to asthenospheric upwelling and partial melting of the mantle source (Wang et al., 2014; Zhao et al., 2018; Zhou et al., 2021). In summary, these mafic rocks provide a unique perspective for studying crustal material recycling and geodynamic processes in orogenic belts.

Mafic magma also plays a significant role in the formation of intermediate (diorite/andesite) magma in orogenic belts through processes that typically involve a combination of magma mixing, fractional crystallization, and crustal assimilation, as seen in examples such as the North Qaidam Orogenic Belt (Chen et al., 2018). In the NQOB, the coexistence of oceanic- and continental-type eclogites confirms that both oceanic and continental crust subducted to mantle depths, along with prior mafic magmatism. This mafic magma led to the formation of intermediate and acidic rocks through various processes (Niu et al., 2021). Consequently, in many areas of the NQOB, interfaces are observed between gabbro, diorite, and granite, etc. As a result, many scholars have debated the evolution of the NQOB, particularly the timing of the transition from oceanic to continental subduction (Chen et al., 2009; Song et al., 2009a; Zhang et al., 2013; Song et al., 2014; Sun et al., 2018; Cai et al., 2021; Niu et al., 2021). On the other hand, while many studies have focused on UHP metamorphic rocks, comprehensive research on mafic rocks—including their chronology, geochemistry, and relationship to UHP metamorphism—has been lacking. This gap has limited our understanding of the nature of the mantle and the geodynamic processes in the NQOB (Song et al., 2003a; Mattinson et al., 2006; Zhang G. et al., 2009; Zhang et al., 2011; Zhang et al., 2013; Song et al., 2014; Zhang G. B. et al., 2016; Chen et al., 2018).

In the NQOB, mafic-intermediate rocks are distributed across Yuka, Luliangshan, Xitieshan, Dulan, Wulan, and the Oulongbuluke terrane, exhibiting varying geochemical characteristics and ages ranging from 535 Ma to 360 Ma (Zhu et al., 2015; Wang et al., 2014; Zhao et al., 2018; Chen et al., 2019; Zhou et al., 2019; Chen et al., 2020; Gao et al., 2021). The main objective of this study is to investigate the timing, geochemical characteristics, and tectonic significance of Paleozoic multi-stage magmatism within the Yuka Terrane of the NQOB, with a focus on mantle modification, tectonic evolution, and associated geodynamic processes.

2 Geological setting

The NQOB is located at the northeastern margin of the Qinghai-Tibet Plateau in northwestern China, at the junction of Qilian block, Qaidam block and Tarim block (Figure 1A), which was formed by the subduction of the Proto-Tethyan ocean beneath the Qilian block and the collision between the Qaidam block and the Qilian block in Paleozoic (Song et al., 2005; Song et al., 2006;

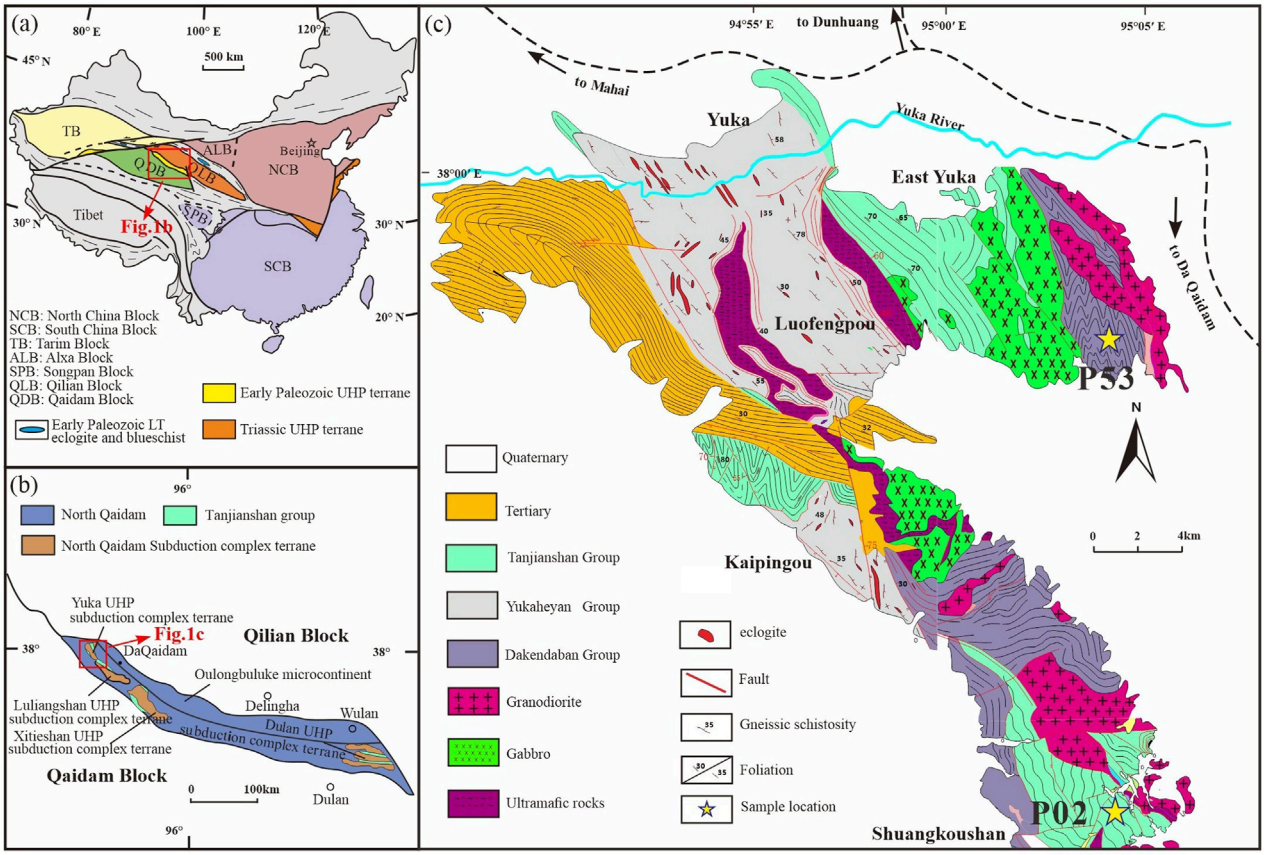

FIGURE 1
(A) The geological map showing the location of the NQOB in Northwest China (modified after Chen et al., 2022a); **(B)** The distribution of the Dulan, Xitieshan, Luliangshan, and Yuka subduction complex terranes (modified after Chen et al., 2022a); **(C)** Showing the geological map of Yuka terrane with sampling locations (modified after Chen et al., 2022a).

Zhang G. B. et al., 2008; Zhang et al., 2013; Song et al., 2014; Yu et al., 2019; Lu et al., 2020). The NQOB extends toward the NWW for ~400 km, bounded by the large sinistral strike-slip Altyn-Tagh fault to the west and a small fault of Wahongshan-Wenquan to the east (Figure 1A). The NQOB mainly includes an UHP metamorphic belt and its northern Oulongbuluke microcontinent (Figure 1B). The Oulongbuluke microcontinent is composed of Paleoproterozoic-Mesoproterozoic metamorphic basement with a Mesoproterozoic-Phanerozoic sedimentary cover (Lu et al., 2008; Chen et al., 2013; Wang et al., 2016; Liao et al., 2018; Wang et al., 2018). It was intruded by early Paleozoic magmatic rocks, such as gabbro, diabase, and diorite (Table 2), which was related to the subduction of the Proto-Tethyan Ocean.

The UHP metamorphic belt includes four HP-UHP subduction complex terranes (Figure 1B; Dulan, Xitieshan, Luliangshan and Yuka) (Chen et al., 2005; Mattinson et al., 2006; Shi et al., 2006; Song et al., 2006; Yang et al., 2006; Zhang et al., 2009b; Zhu et al., 2010; Song et al., 2014; Zhao et al., 2017; Sun et al., 2018; Chen et al., 2019; Song et al., 2019; Gao et al., 2021; Niu et al., 2021; Zhou et al., 2021). The HP-UHP metamorphic rocks primarily consist of HP metagranitic and metapelitic gneiss, interspersed with smaller amounts of eclogite, garnet peridotite, and mafic granulite (Yang et al., 2001; Song et al., 2003b; Song et al., 2006; Yang et al., 2006; Song et al., 2007; Zhang J. et al., 2008; Song et al., 2009b; Zhang et al., 2009c; Yu et al., 2013; Chen et al., 2018). Eclogites in the form of lenses, blocks, and layers are distributed in paragneiss and orthogneiss at Yuka, Xitieshan and Dulan, and their UHP metamorphic age of 460-420Ma has been recorded (Table 1). The discovery of coesite inclusions in eclogite and paragneiss, as well as diamond inclusions in garnet peridotite, provides evidence of UHP metamorphism and the deep subduction of the Qaidam block (Yang et al., 2001; Song et al., 2003a; Song et al., 2005; Zhang G. et al., 2009). In addition, magmatic rocks formed during the orogenic process are also widely exposed in the belt, including arc-like volcanic-igneous rocks, basic-ultrabasic intrusive rocks, ophiolite, granitic intrusive rocks, and felsic dykes, which are interpreted as being related to the subduction of the South Qilian oceanic and post-orogenic (Wu et al., 2007; Chen et al., 2012; Wang et al., 2014; Wu T. et al., 2014; Zhu et al., 2014; Zhang et al., 2015; Zhao et al., 2017; Sun et al., 2018; Chen et al., 2019; Wu et al., 2019; Chen et al., 2020; Gao et al., 2021; Zhou et al., 2021; Chen et al., 2025). Volcano-igneous rocks include basalt, basaltic andesite, andesite, and rhyolite, etc., they have arc-related geochemical features and zircon U-Pb crystallization ages range from 520 Ma to 445 Ma (Tables 1, 2), which are interpreted as related to the development of island arc or back-arc setting. In summary, comprehensive chronological and

geochemical studies of these rocks show that the North Qaidam experienced a complex tectonic evolutionary history, including the opening of an oceanic basin, ocean-continent subduction, continent-continent collision, and the exhumation of a subducted slab during the Paleozoic (Song et al., 2009a; Song et al., 2009b; Zhang et al., 2013; Song et al., 2014; Zhu et al., 2014; Song et al., 2015; Zhang L. et al., 2016; Sun et al., 2018).

The Yuka terrane is one of the most significant components of the NQOB (Figure 1C). Located in the northwest of the UHP metamorphic belt, it primarily comprises the Tanjianshan Group rocks, Yukahe Group rocks, Dakendaban Group rocks, granodiorite, gabbro, and ultrabasic rocks. The Yukahe Group mainly consists of granitic gneiss, argillaceous schist, and argillaceous gneiss, which are in fault contact with the early Paleozoic Island arc volcanic-sedimentary rocks, dunite, and Cambrian gabbro of the Tanjianshan Group (Chen et al., 2007; Chen et al., 2009; Zhang et al., 2009b; Ren et al., 2017; Ren et al., 2019).

Eclogites in the Yukahe Group occur as layered or lenticular blocks, and their retrograde metamorphism is minimal, allowing reliable UHP metamorphic ages to be obtained (Table 1; 436–431 Ma). These ages are later than the arc-back arc magmatism associated with the subduction of the oceanic slab in the region (Table 1; 446 Ma).

The Dakendaban Group dates to the Proterozoic and is dominated by intermediate metamorphic plagioclase-amphibolite, with minor magmatic intrusions (Lu et al., 2002; Zhou et al., 2019). In contrast, the Tanjianshan Group consists of a suite of greenschist facies and severely deformed rocks, representing a significant Early Paleozoic volcanic-sedimentary formation (Li et al., 2006).

The magmatic rocks of the Dakendaban and Tanjianshan Groups in the terrane are better preserved than those in other areas, making them particularly suitable for addressing the research gaps identified in previous studies.

3 Sampling and petrography

In this study, rock samples (P02 and P53) were collected from the Dakendaban and Tanjianshan Groups of the Yuka terrane (Figure 1C). The outcrops of these two groups indicate that they have undergone later alteration (Figure 2). Eight of the freshest samples were selected for testing and analysis. The P02 gabbro samples, collected from the Tanjianshan Group, include P02G4-1, P02G4-2, P02G4-3, and P02G19-1. The intrusion was in fault contact with the Tanjianshan Group. The P53 diorite samples, collected from the Dakendaban Group, include P53G3-1, P53G5-1, P53G6-1, and P53G6-2. The intrusion was in intrusive contact with the Dakendaban Group. The characteristics of the petrographic observations are as follows.

The P02 gabbros are light grey-black with a gabbro-diabase texture and a massive outcrop. They are primarily composed of plagioclase (50± vol%), clinopyroxenes (25± vol%), and hornblende (20± vol%), with minor amounts of quartz (1± vol%), biotite (1± vol%), a few opaque minerals (1± vol%), and tiny amounts of chlorite (Figures 2A, B, E, F). Plagioclase is subhedral to anhedral with grain sizes of 0.2–0.6 mm and shows well-developed polysynthetic twinning. Clinopyroxenes is subhedral with grain sizes of 0.2–1.5 mm, distributed in the interstice of plagioclase. Hornblende is subhedral with grain sizes of 0.3–1.4 mm. Some photomicrographs show minor alteration, such as hornblendization of clinopyroxenes (Figures 2E, F).

The P53 diorites are also massive outcrop with grey-black in color and texture similar to gabbro-diabase. They are primarily composed of plagioclase (65± vol%), hornblende (25± vol%), pyroxene (3± vol%), and biotite (2± vol%), with minor amounts of quartz (1± vol%) and opaque minerals (1± vol%), along with trace amounts of chlorite (Figures 2C, D, G, H). Plagioclase is subhedral to anhedral with grain sizes of 0.1–0.8 mm and shows well-developed polysynthetic twinning. Hornblende is subhedral with grain sizes of 0.2–1.2 mm. Pyroxene and biotite are subhedral with grain sizes of 0.1–0.3 mm, distributed in the interstice of plagioclase. Some photomicrographs show minor alteration, such as chloritization (Figures 2G, H).

4 Analytical methods

Eight selected samples from both groups were used for whole-rock major and trace element analysis, as well as Sr-Nd isotope analysis. Zircons from two samples (P02G19-1 and P53G3-1) were selected for U-Pb dating and trace element analysis.

4.1 Zircon U-Pb geochronology and trace elements analysis

The samples were washed, and crushed into fine powder by jaw crusher at the Regional Geological Survey Research Institute of Langfang City, Hebei Province. Zircon grains were extracted by sieving, and standard heavy-liquid and magnetic separation techniques, then were selected following examination with a binocular microscope. The selected zircons were sent to Wuhan Sample Solution Analytical Technology Co., Ltd. for target preparation, mounted in epoxy resin, polished to approximately one-third of their thickness, and imaged using a cathodoluminescence (CL) detector with a scanning electron microscope (JEOL). Zircon U-Pb isotopic dating and trace element content analysis was conducted using LA-ICP-MS. The detailed operating conditions for the laser ablation system, ICP-MS instrument, and data reduction procedures followed those described by Zong et al. (2017). The laser spot size and frequency were set to 24 μm and 80 Hz, respectively, and the laser ablation depth was 20–40 μm. Zircon 91,500 and glass NIST610 were used as external standards for U-Pb dating and trace element calibration, respectively. Each analysis was performed using a background acquisition of approximately 20–30 s, followed by 50 s, of data acquisition. The offline processing of analysis data was completed by ICP-MS-DataCal software, including selection of background and analysis signal, instrument sensitivity drift correction, trace element analysis, U-Pb isotope ratio and age calculation, etc., (Liu et al., 2008a; Liu et al., 2010). The calculation of zircon U-Pb age weighted mean value and the Concordia diagrams were completed by Isoplot software (Ludwig, 2003).

TABLE 1 Ages of oceanic and continental crust HP/UHP metamorphism and arc-back arc magmatism in the North Qaidam Orogenic Belt.

Rock type	Sample no.	Age of metamorphism (Ma)	Age of protolith (Ma)	Region	Method	References
Age of HP/UHP metamorphism related to oceanic subduction						
Eclogite	2D155	457 ± 7		Dulan terrane	SHRIMP	Song et al. (2006)
Eclogite	2D73	462 ± 13		Dulan terrane	SHRIMP	Song et al. (2014)
Grt-pyroxenite	4C19	450 ± 11		Dulan terrane	SHRIMP	Song et al. (2014)
Eclogite	99Y115	458 ± 10		Dulan terrane	Sm-Nd	Song et al. (2003a)
Eclogite	99Y313	459 ± 3		Dulan terrane	Sm-Nd	Song et al. (2003b)
Eclogite	D5A	449 ± 2		Dulan terrane	SHRIMP	Mattinson et al. (2006)
Eclogite	D5B	442 ± 7		Dulan terrane	SHRIMP	Mattinson et al. (2006)
Eclogite	5S23	445 ± 7	516 ± 8	Dulan terrane	SHRIMP	Zhang J. et al. (2008)
Eclogite	7X368	461 ± 4		Xitieshan terrane	SHRIMP	Zhang et al. (2011)
Grt-dunite	2C39	446 ± 13		Lüliangshan	SHRIMP	Song et al. (2005)
Grt-lherzolite	C305	457 ± 22		Lüliangshan	SHRIMP	Song et al. (2005)
Age of HP/UHP metamorphism related to continental subduction						
Eclogite	D5B	433 ± 5		Dulan terrane	SHRIMP	Mattinson et al. (2006)
Eclogite	D3F	422 ± 4		Dulan terrane	SHRIMP	Mattinson et al. (2006)
Eclogite	Q08-20-3.1	430 ± 4		Dulan terrane	SHRIMP	Zhang et al. (2009a)
Eclogite	Q07-8-2.2	438 ± 2	~835	Dulan terrane	SHRIMP	Zhang et al. (2009b)
Eclogite	Q08-10-5.1	446 ± 10	~835	Dulan terrane	LA-ICPMS	Zhang et al. (2009c)
Eclogite	2D73	424 ± 13		Dulan terrane	SHRIMP	Song et al. (2014)
Eclogite	4C04	425 ± 8		Dulan terrane	SHRIMP	Song et al. (2014)
garnet pyroxenite	4C19	425 ± 9		Dulan terrane	SHRIMP	Song et al. (2014)
Eclogite	7×2–7	439 ± 8	~870	Xitieshan terrane	SHRIMP	Zhang et al. (2011)
Eclogite	Q7-15	433 ± 3		Xitieshan terrane	SIMS	Song et al. (2012)
Eclogite	04QH11	431 ± 4	795–748	Yuka terrane	LA-ICPMS	(Chen et al., 2009)
Eclogite	04QH14	436 ± 3	793–783	Yuka terrane	LA-ICPMS	(Chen et al., 2009)
Eclogite	9C16	408–439	856	Yuka terrane	LA-ICPMS	Zhang G. B. et al. (2016)
Eclogite	9C42	431 ± 5		Yuka terrane	LA-ICPMS	Zhang L. et al. (2016)
Eclogite	9C58	436 ± 5	875	Yuka terrane	LA-ICPMS	Zhang G. B. et al. (2016)
Eclogite	4Y04	433 ± 20	~850	Yuka terrane	SHRIMP	Song et al. (2010)
Eclogite	2C87		~850	Yuka terrane	SHRIMP	Song et al. (2010)
Grt-lherzolite	C305	423 ± 6		Lüliangshan	SHRIMP	Song et al. (2005)

(Continued on the following page)

TABLE 1 (*Continued*) Ages of oceanic and continental crust HP/UHP metamorphism and arc-back arc magmatism in the North Qaidam Orogenic Belt.

Rock type	Sample no.	Age of metamorphism (Ma)	Age of protolith (Ma)	Region	Method	References
Grt-harzburgite	2C39	420 ± 6		Lüliangshan	SHRIMP	Song et al. (2005)
Grt-lherzolite	07SLK02	427 ± 3		Lüliangshan	LA-ICPMS	Xiong et al. (2011)
Grt-pyroxinite	07SLK05	429 ± 3		Lüliangshan	LA-ICPMS	Xiong et al. (2011)
Age of arc-back arc magmatism related to oceanic subduction						
Dacite Andesite Basic volcanic rock	XTS-71–2 ZJG-18–2 ZJG-24–2 XTS-63–2	454 ± 6		Xitieshan	LA-ICPMS	Sun et al. (2018)
Gabbro Diorite-porphyrite Basaltic andesite Epidiorite	XTS-103–2 XTS-97–2 ZJG-47–2 ZJG-51–2	458 ± 3		Xitieshan	LA-ICPMS	Sun et al. (2018)
Volcanic rock	DQY-35	514 ± 9			SHRIMP	Shi et al. (2006)
Basic volcanic rock	ZJ18-1	464 ± 4		Xitieshan	LA-ICPMS	Liang et al. (2014)
Acid volcanic rock	XTS04-1	458 ± 4		Xitieshan	LA-ICPMS	Fu et al. (2017)
Basic volcanic rock	XTS17-2	462 ± 4		Xitieshan	LA-ICPMS	Fu et al. (2017)
Rhyolite porphyry	XTS16-1	454 ± 6		Xitieshan	LA-ICPMS	Fu et al. (2017)
Gabbro		468–522		Dulan	LA-ICPMS	Zhu et al. (2010)

4.2 Whole-rock major and trace elements analysis

Whole-rock major and trace element concentrations were obtained using X-ray fluorescence (XRF), atomic absorption spectrometry (AAS), and inductively coupled plasma mass spectrometry (ICP-MS). Major elements were analyzed at the Mineral Resources Analyzing Center of the Ministry of Land and Resources, Wuhan, using XRF and AAS, with analytical uncertainties below 5%. Trace elements were analyzed at the State Key Laboratory of China University of Geosciences using ICP-MS (Agilent 7500a with a shield torch). Rare earth elements (REEs) were separated by cation-exchange techniques. Analytical uncertainties ranged from 1% to 3%. The analytical results for the BHVO-1 (basalt), BCR-2 (basalt), and AGV-1 (andesite) standards indicated that the trace elements' precision was N10%. A detailed description of the experimental methods can be found in Liu et al. (2008b) and Rudnick et al. (2004).

4.3 Whole-rock Sr-Nd isotopic analysis

Whole-rock Sr-Nd isotopic compositions were measured using a Triton thermal ionization mass spectrometer (TIMS) at Sample Solution Analytical Technology Co., Ltd. The Sr-Nd isotopic analytical techniques are described in detail by Liu et al. (2008a). The exponential law, initially developed for TIMS measurement (Russell et al., 1978) and widely accepted for use in MC-ICP-MS, was applied to assess instrumental mass discrimination in this study. Mass discrimination correction was performed via internal normalization to an $^{88}Sr/^{86}Sr$ ratio of 8.375209 and a$^{146}Nd/^{144}Nd$ ratio of 0.7219 (Lin et al., 2016). The interference-related elements Sm, Ca, Rb, Er, and Yb were completely separated using ion-exchange resins. Remaining interferences from $^{144}Sm^{+}$, $^{83}Kr^{+}$, $^{85}Rb^{+}$, $^{167}Er^{2+}$, and $^{173}Yb^{2+}$ were corrected based on the method described by Lin et al. (2016). The USGS reference materials BCR-2 (basalt) and RGM-2 (rhyolite) were consistent with their published values (Li et al., 2012). The CHUR composition used to calculate the εNd(t) values was $^{143}Nd/^{144}Nd = 0.512638$ and $^{147}Sm/^{144}Nd = 0.196$ (Bouvier et al., 2008), with a decay constant of 6.54×10-12. Nd model ages were calculated according to the depleted mantle model of Liew and Hofmann (1988).

5 Analytical results

5.1 Zircon U-Pb geochronology and trace elements

The zircon U-Pb age and trace element analysis results of the two samples (P02G19-1 and P53G3-1) are shown in

TABLE 2 U-Pb zircon ages of intermediate-mafic rocks in the North Qaidam region, NW China.

Sample no.	Plutons and their locations	Rocks	Ages (Ma)	References	Geochemical compositions
09QH19	Dulan	gabbro	837 ± 3	Zhu et al. (2015)	E-MORB
99Y	Lüliangshan	basaltic rock	780 ± 22	Yang et al. (2004)	MORB
14QH-21	Lüliangshan	gabbro	535 ± 2	Chen et al. (2020)	FAB
14QH-22	Lüliangshan	gabbro	513 ± 3	Chen et al. (2020)	FAB
16QH-48	Lüliangshan	gabbro	510 ± 3	Chen et al. (2020)	FAB
09QH27	Lüliangshan	gabbro	535 ± 2	Zhu et al. (2014)	N-MORB
09QH8	Xitieshan	gabbro	521 ± 7	Zhu et al. (2012)	OIB
WL18-3-8	Oulongbuluke block	gabbro	490 ± 4	Gao et al. (2021)	OIB
WL18-2-9.3	Oulongbuluke block	gabbro	487 ± 5	Gao et al. (2021)	OIB
WL18-3-1	Oulongbuluke block	gabbro	487 ± 3	Gao et al. (2021)	OIB
WL18-2-9.4	Oulongbuluke block	gabbro	485 ± 4	Gao et al. (2021)	OIB
10QH1	Dulan	gabbro	480 ± 1	Zhu et al. (2015)	OIB
P02G19-1	Yuka	gabbro	471 ± 3	(The study)	arc-like
03Q01/06Q	Dulan	gabbro	468 ± 2	Zhu et al. (2010)	arc-like
HDS-ZK001-N20	Oulongbuluke block	gabbro	466 ± 1	Li et al. (2019)	arc-like
HDS-DB-N2	Oulongbuluke block	pyroxenite	455 ± 4	Li et al. (2019)	arc-like
P7TW13-4	Lüliangshan	basaltic andesite	432 ± 6	Zhou et al. (2019)	MORB
CHH39	Wulan Chahanhe	diorite	441 ± 2	Niu et al. (2021)	arc-like
P53G3-1	Yuka	diorite	438 ± 3	(The study)	arc-like
CHH09	Wulan Chahanhe	diabase	429 ± 4	Niu et al. (2021)	arc-like
CHH18	Wulan Chahanhe	gabbro	441 ± 5	Niu et al. (2021)	E-MORB
CHH47	Wulan Chahanhe	gabbro	439 ± 5	Niu et al. (2021)	E-MORB
07SLK25	Lüliangshan	pyroxenite Dyke	401 ± 7	Xiong et al. (2014)	arc-like
9C-67	Dulan	intermediate dyke	393 ± 1	Zhou et al. (2021)	arc-like
Q14-14	Dulan	intermediate dyke	380 ± 5	Zhou et al. (2021)	arc-like
18CB-28	Dulan	basic dyke	383 ± 1	Zhou et al. (2021)	arc-like
18CB-83	Xitieshan	basic dyke	375 ± 3	Zhou et al. (2021)	arc-like
18CB-84	Xitieshan	gabbro	368 ± 3	Zhou et al. (2021)	arc-like
B1204-1	Xitieshan	gabbro	372 ± 2	(Zhao et al., 2018	arc-like
07DL-55	Dulan Yematan	diorite	360 ± 4	Wang et al. (2014)	arc-like
10DL-24	Dulan Yematan	diorite	374 ± 2	Wang et al. (2014)	arc-like

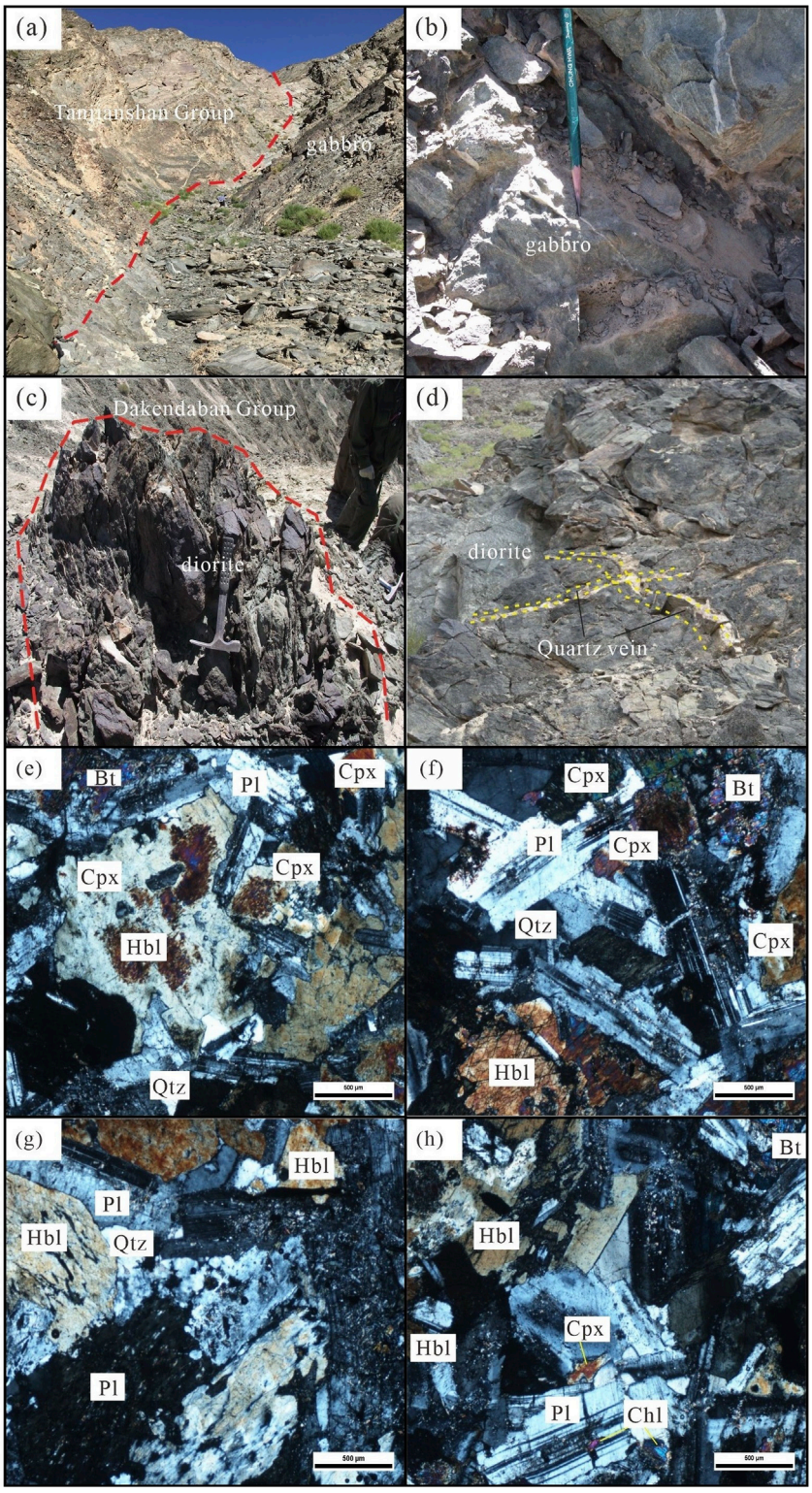

FIGURE 2
Representative field photographs and photomicrographs of representative samples (P02-gabbro and P53-diorite) from Yuka terrane: **(A)** P02 gabbro intrudes into the early Paleozoic Tanjianshan Group; **(B)** Field photographs of P02 gabbro; **(C)** P53 diorite intrudes into the Proterozoic Dakendaban Group; **(D)** Field photographs of P53 diorite; **(E, F)** Representative micrographs of P02 gabbro, showing a mineral assemblage of plagioclase, pyroxene, hornblende, and minor quartz and biotite; **(G, H)** Representative micrographs of P53 diorite, characterized by weak plagioclase alteration, hornblende, pyroxene, and minor quartz and biotite.

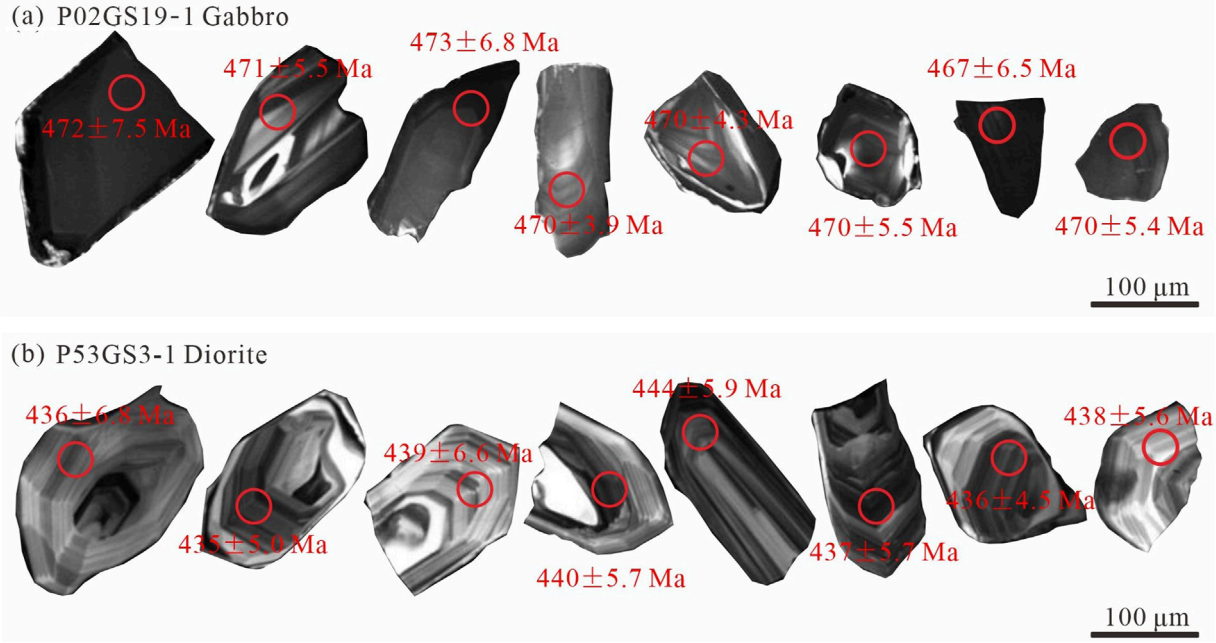

FIGURE 3
Representative cathodoluminescence (CL) images of zircon grains from sample **(A)** P02G19-1 and **(B)** P53G-three to one, the red circles show the locations of U-Pb analyses.

Supplementary Tables S1, S2. The Concordia diagram of zircon U-Pb ages and the diagram of Chondrite-normalized REE patterns for zircon are shown in Figure 4.

Typical CL images of sample P02G19-1 and P53G3-1 (Figure 3) indicate that the zircons are fresh and have undergone very little late alteration. Grains exhibiting typical magmatic zircon characteristics were selected for analysis. The zircons of sample P02G19-1 are mostly long columnar and equiaxed, with grain sizes generally ranging from 50–150 μm and length to width ratios of 1:1 to 2:1, obvious tabular zone and weak oscillating zone (Figure 3A). Zircon analysis results show high content of total REE (ΣREE = 2,683–7,540 ppm), U (4,178–19578 ppm) and Th (2,331–6,579 ppm) with obvious fractionation of LREE and HREE (LREE/HREE: 0.4–0.14) (Supplementary Figure S4b; Supplementary Tables S1, S2). The mean value of Th/U ratio is 0.69 > 0.5, steep HREE pattern and significant positive Ce anomaly (Supplementary Figure S4b; Supplementary Table S1), these indicate that the zircons of sample P02G19-1 are of magmatic origin (Corfu et al., 2003; Hoskin and Schaltegger, 2003; Wu and Zheng, 2004). Eighteen analyses from zircons of P02G19-1 yield concordant $^{206}Pb/^{238}U$ ages ranging from 471 to 467 Ma (Supplementary Table S1). The weighted mean of 470.6± 3.1 Ma (MSWD = 0.037; n = 18) is interpreted as the crystallization age of the gabbro (Figure 4A).

The zircons of sample P53G3-1 are mostly short-columnar and a few long-columnar, with grain sizes ranging from 50 to 200 μm and length/width ratios of 1:1 to 2:1, and obvious oscillating zone (Figure 3B). Zircon analysis results show that there is a variable content of total REE (ΣREE = 1,078–7,813 ppm), U (304–2,294 ppm) and Th (229–1,060 ppm) with obvious fractionation of LREE and HREE (LREE/HREE: 0.004–0.096) (Supplementary Figure S4D; Supplementary Tables S1, S2). The mean value of Th/U ratio is 0.51 > 0.5, steep HREE pattern, obvious negative Eu anomaly and positive Ce anomaly (Supplementary Figure S4D; Supplementary Table S1), these indicates that the zircons of sample P53G3-1 are of magmatic origin (Corfu et al., 2003; Hoskin and Schaltegger, 2003; Wu and Zheng, 2004). Seventeen analyses from zircons of sample P53G3-1 yield concordant $^{206}Pb/^{238}U$ ages ranging from 449 to 433 Ma (Supplementary Table S1). The weighted mean of 438.4± 2.9 Ma (MSWD = 0.52; n = 17) is interpreted as the crystallization age of the diorite (Figure 4C).

5.2 Whole-rock major and trace elements

Eight samples were selected for major and trace element analyses, and results are presented in Supplementary Table S3. P02 samples have low loss-on-ignition (LOI) values, and P53 samples have high loss-on-ignition (LOI) values, and its influence on rock composition will be discussed later. In the total alkali-SiO_2 and Nb/Y - Zr/(TiO_2*0.0001) diagrams, the eight samples belong to the subalkaline series, the P02 fall into the gabbro fields, and the P53 fall into the gabbro or gabbroic-diorite fields (Figures 5A, B).

Samples P02 have small variations in SiO_2 contents that range from 45.34 to 49.95 wt%, with high contents of CaO = 8.71–11.20 wt% (mean = 10.45 wt%), FeO = 7.10–9.30 wt% (mean = 8.10 wt%), MgO = 7.14–8.66 wt% (mean = 7.58 wt%, $Mg^{\#}$ values [100 × molar MgO/(MgO + FeO)] of 49–55), Al_2O_3 = 12.53–13.77 wt% (mean = 13.41 wt%) and FeO^T (10.4–16.3 wt%), indicating that they have the property of strong mafic rocks. In addition, these gabbros have low contents of Na_2O = 1.86–2.47 wt% (mean = 2.10 wt%), K_2O

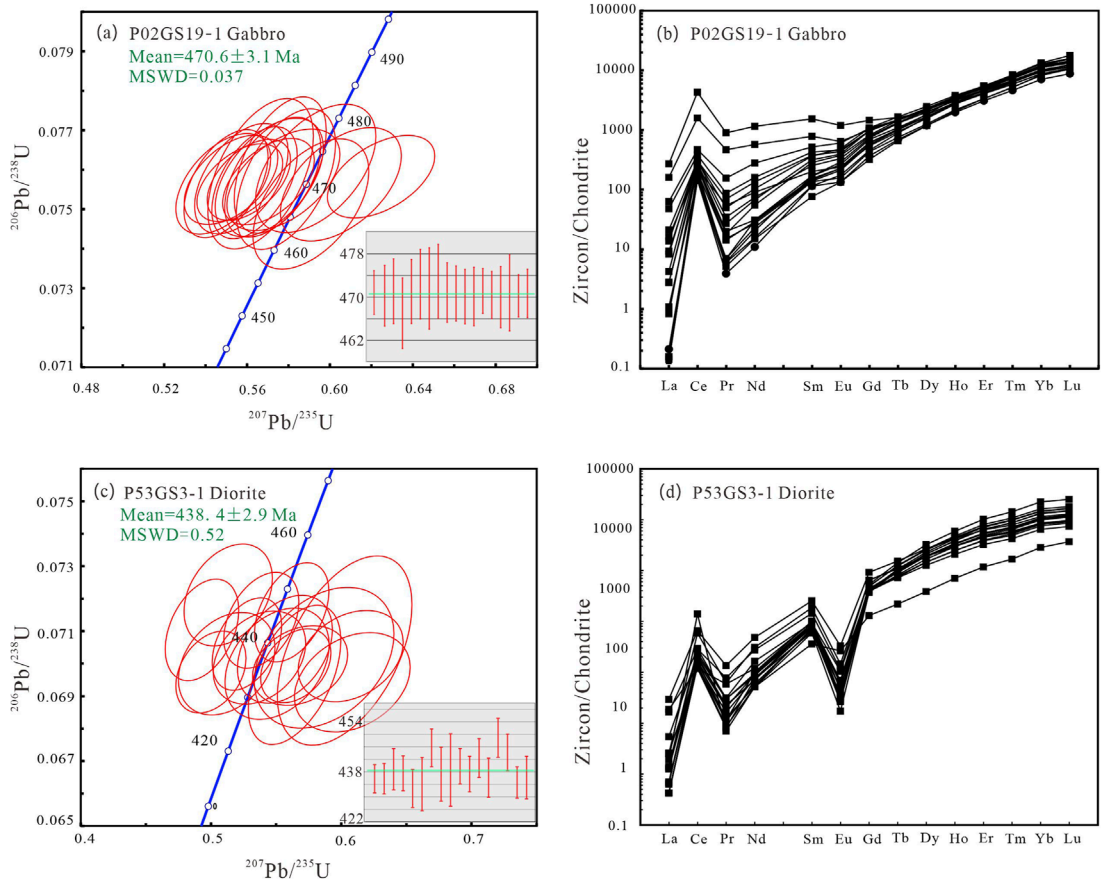

FIGURE 4
(A, C) U-Pb Concordia diagrams and **(B, D)** chondrite-normalized REE patterns of zircon from the gabbro (P02G19-1) and the diorite (P53G3-1). Chondrite-normalization values are taken from Sun and McDonough (1989).

= 0.81–1.62 wt% (mean = 1.31 wt%), P_2O_5 = 0.23–0.45 wt% (mean = 0.29 wt%) and TiO_2 (0.61–1.34 wt%).

Samples P53 have moderate variations in SiO_2 contents that range from 50.06 to 56.24 wt%, highly variable contents of CaO = 4.38–12.51 wt% (mean = 8.22 wt%), MgO = 2.73–9.62 wt% (mean = 5.44 wt%, $Mg^{\#}$ values [100 × molar MgO/(MgO + FeO)] of 39–67) and Al_2O_3 = 11.47–16.07 wt% (mean = 14.08 wt%). In addition, these diorites have low contents of FeO = 4.15–5.80 wt% (mean = 5.11 wt%, FeO^T of 7.5–8.6 wt%), Na_2O = 1.95–5.78 wt% (mean = 4.07 wt%), K_2O = 0.16–2.23 wt% (mean = 0.84 wt%) and TiO_2 (0.52–0.91 wt%). These indicate that they also have the property of mafic rocks.

In terms of whole-rock trace elements, two groups of rocks show similar characteristics. All samples exhibit enrichment in light rare earth elements (LREE) relative to HREE in the chondrite-normalized REE diagram, distributed between OIB and E-MORB (Figures 6A, C). In the primitive mantle-normalized trace elements spider diagram (Figures 6B, D), all samples display enrichment in large-ion lithophile elements (LILE: Rb, Ba and K) and radioactive elements (Th and U), and depletion in high field strength elements (HFSE: Nb, Ta, Zr, Hf and Ti). Samples P02 have relatively high total rare earth elements (ΣREE = 117.35–160.07 ppm), LREE/HREE ratio (5.36–9.90), and $(La/Yb)_N$ ratio (5.5–13.7), indicating obvious fractionation of LREE and HREE (Supplementary Table S3). Samples P53 have relatively high total rare earth elements (ΣREE = 109.74–148.76 ppm) and LREE/HREE ratio (7.22–10.43, $(La/Yb)_N$ value of 7.4–13.2), indicating obvious fractionation of LREE and HREE. All samples show consistent weak negative Eu anomalies (δEu = 0.74–0.86), no anomalies of Ce (δCe = 0.94–1.02) and high positive anomalies of Pb (Supplementary Table S3; Figure 6). In addition, the contents of large ion lithophile elements (LILE) such as Rb, Ba and K in samples P53 are lower than those in samples P02, and the contents of high field strength elements (HFSE) such as Nb, Ta, Zr and Hf in P53 are higher than those in P02 (Supplementary Table S3). In summary, these results indicate that the two groups of rocks have arc-like trace element compositions similar to those of island arc volcanic rocks (Figure 6).

5.3 Whole-rock Sr-Nd isotopic analysis

Eight samples were selected for Sr-Nd isotopic analyses, according to the zircon U-Pb dating results of samples P02G19-1 and P53G3-1, the initial isotopic ratios of Sr, Nd, εSr(t), εNd(t), $T_{DM}(Nd)$ and $T_{DM2}(Nd)$ were calculated (Supplementary Table S4).

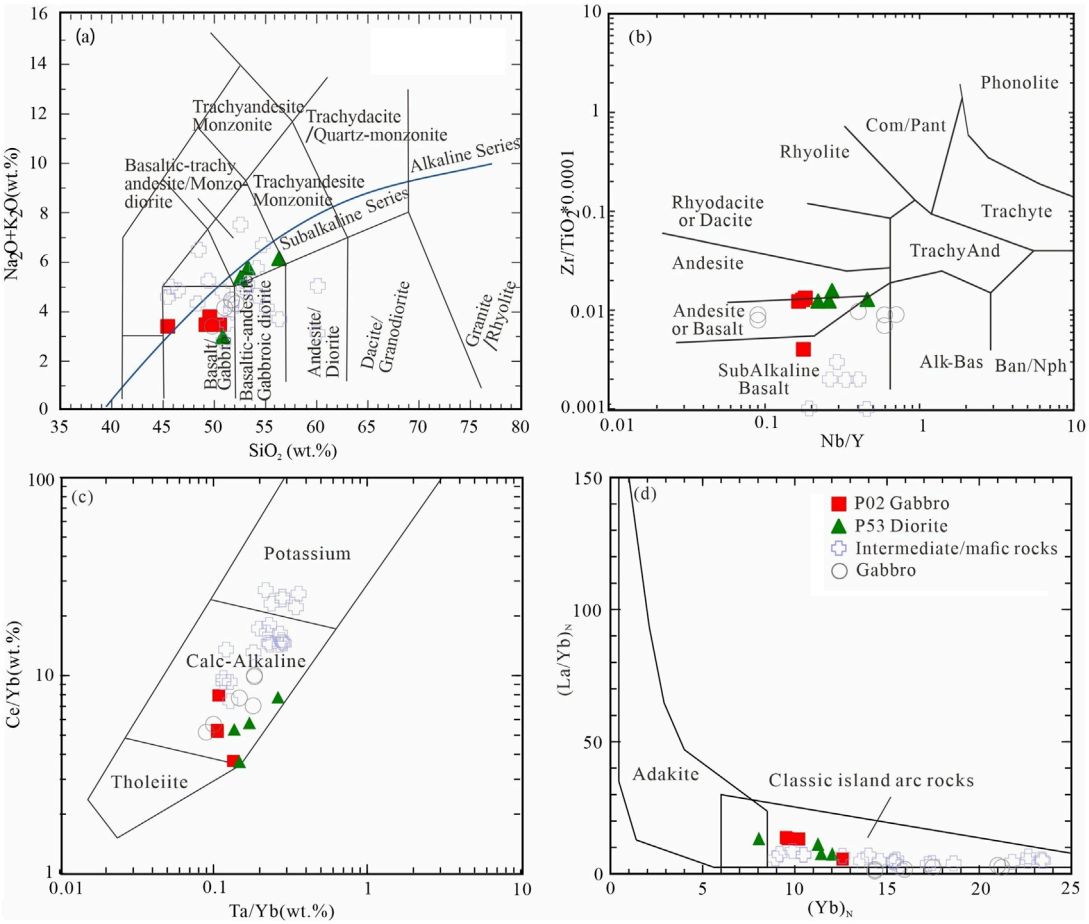

FIGURE 5
The discrimination diagram of rock types/series for P02 and P53 from Yuka area. Post-collisional intermediate-mafic rocks and gabbro from Zhao et al. (2017) and Zhou et al. (2021) (grey circle and light purple cross). **(A)** SiO_2 vs Na_2O+K_2O (after Le Maitre et al., 1989),blue trend line from Irvine and Baragar, (1971). **(B)** Nb/Y vs Zr/TiO_2 (after Winchester and Floyd, 1977). **(C)** Ta/Yb vs Ce/Yb diagram (after Pearce, 1982) for samples. **(D)** $(Yb)_N$ vs. $(La/Yb)_N$ (after Hansen et al., 2002).

Samples P02 and P53 display variable $(^{87}Sr/^{86}Sr)_i$ ratios ranging from 0.70473 to 0.70811 (mean = 0.70566) and 0.70599 to 0.70685 (mean = 0.70631), with εNd(t) values ranging from −2.7 to +0.3 and −1.0 to +1.5, respectively. Their T_{DM2}(Nd) ages are 1,164–1,429 Ma for P02 and 1,063–1,270 Ma for P53 (Supplementary Table S4). These results indicate that the rocks exhibit arc-like compositional characteristics, falling within the mantle array and enriched subcontinental lithospheric mantle (E-SCLM) of the NQOB (Figure 7).

6 Discussion

6.1 Sources and petrogenesis

Primary mafic magmas provide valuable insights into the composition of their mantle sources. However, the geochemical composition of rocks formed from these magmas is influenced not only by the mantle source but also by open-system processes. Fractional crystallization, an open-system process, generally does not significantly modify the isotopic composition of a system, as isotopic fractionation during this process is typically very small. Therefore, the effects of open-system processes on the composition of the primary magmas must be evaluated before drawing conclusions about the nature of the mantle sources.

6.1.1 Key open-system processes affecting primary mafic magmas

The later alteration may have influenced the concentrations of certain elements and isotope compositions, particularly for water-soluble elements such as LILE and LREE (Zhao and Zhou, 2007; Khan et al., 2024). The Yuka Terrane rock samples (P02 and P53) from both groups have undergone weak alteration. LOI (Loss on Ignition), which indicates the degree of alteration, shows values ranging from 1.30 to 2.17 wt% for P02 and from 1.66 to 4.18 wt% for P53 (with one outlier value of 7.08 wt%). These results suggest that both P02 and P53 were minimally affected by alteration.

Furthermore, no correlation is observed between LOI and Rb, Pb, U, or εSr(t) for P02, whereas a weak correlation exists for P53 (Supplementary Figure S1). This indicates that P53

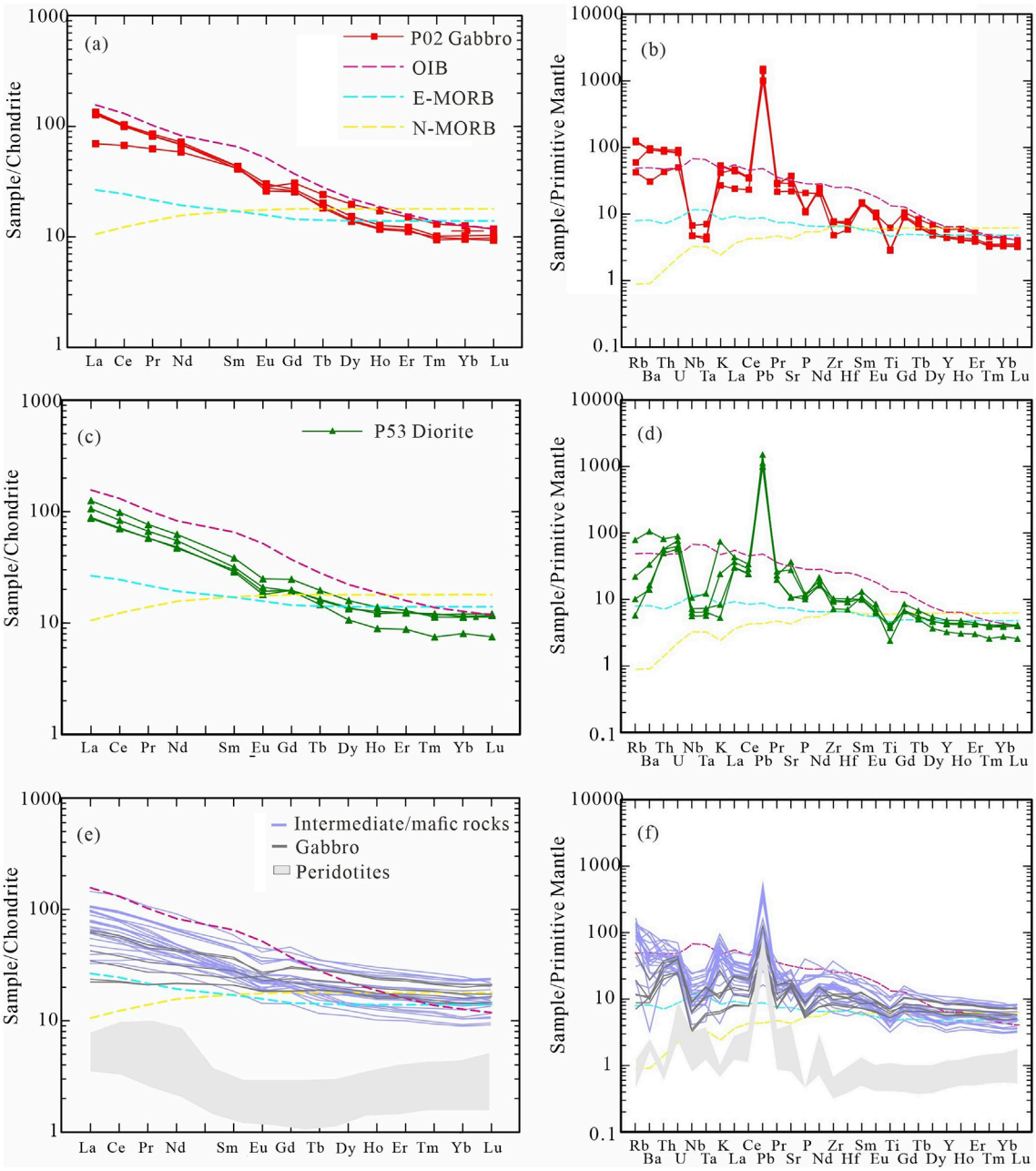

FIGURE 6
(A, C) Chondrite-normalized REE patterns and **(B, D)** primitive mantle-normalized trace element patterns for intermediate-mafic rocks (P53 and P02). Chondrite values are from Boynton et al. (1984). The data for primitive mantle, N-MORB, E-MORB and OIB are from Sun and McDonough (1989). **(E, F)** Post-collisional intermediate-mafic rocks and gabbro from Zhao et al. (2018) and Zhou et al. (2021) and peridotites from Xiong et al. (2015).

was slightly affected by alteration (particularly for mobile elements like Rb), while P02 remained largely unaffected.

Crustal contamination is an important open-system process during ascent and emplacement of magmas (Fang et al., 2019), can introduce crustal materials with high SiO_2, K_2O, Pb, LILE, LREE, radiogenic Sr isotopes and low radiogenic εNd(t) values to mantle-derived magmas (Hans Wedepohl, 1995; Rudnick and Gao, 2003), which will lead to a negative correlation between SiO_2 (or K_2O) and εNd(t), Nb/U and Ce/Pb, and a positive correlation between SiO_2 (or K_2O) and the initial $^{87}Sr/^{86}Sr$ ratios. However, for P02 and P53, there is no significant correlation between K_2O and Nb/U, or between SiO_2 and Ce/Pb, εNd(t), initial $^{143}Nd/^{144}Nd$, and initial $^{87}Sr/^{86}Sr$ (Supplementary Figures S2A, S4B–D). K_2O shows a negative correlation with initial $^{87}Sr/^{86}Sr$ Supplementary Figures S2B, S4A), and εNd(t) values range from weakly negative to weakly positive. Additionally, the ratio of elements with similar partition coefficients is not significantly affected by the degree of fractional crystallization or partial melting. As a result, these correlations can be utilized to assess the extent of crustal contamination. The Nb/Ta ratio of the two groups of rocks ranges from 15.0 to 19.7 (Supplementary Table S3),

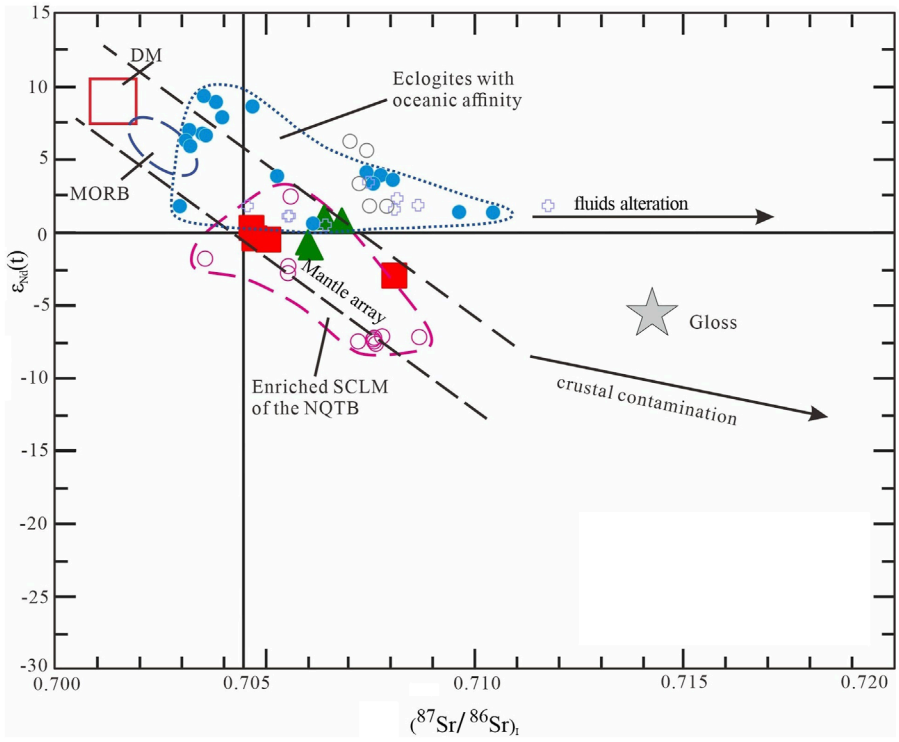

FIGURE 7
Initial Sr-Nd isotopic compositions of intermediate-mafic rocks (P53 and P02) from Yuka area (modified from Niu et al., 2021). Data for subcontinental lithospheric mantle (SCLM) of the North Qaidam tectonic belt are from Xiong et al. (2015). Data for eclogite with oceanic affinities in the North Qaidam tectonic belt are from Zhang et al. (2019) and Zhang L. et al. (2017). The isotopic compositions for MORB and the mantle end-members DM are from Zindler and Hart, (1986), for global subducted sediments (Gloss) are from Plank and Langmuir (1998). Post-collisional intermediate-mafic rocks and gabbro from Zhao et al. (2018) and Zhou et al. (2021) (grey circle and light purple cross). The symbols are the same as in Figure 5.

with an average value of 17.5, which aligns closely with the primary mantle value of 17.4 (Sun and McDonough, 1989). The plots of Nb/Ta versus initial $^{87}Sr/^{86}Sr$ exhibit a positive correlation, whereas Nb/Ta versus initial $^{143}Nd/^{144}Nd$ show no significant correlation (Supplementary Figures S2C, D). These observations indicate that the influence of crustal contamination on rock composition is negligible.

Fractional crystallization is also a crucial process during ascent and emplacement of magmas, and can modify the compositions of mafic to intermediate magmas. For P02, the narrow range of $Mg^{\#}$ value and MgO contents (Supplementary Table S3) indicate that fractionation crystallization was very weak during magma evolution. P02 exhibit no correlation between FeO^T and MgO, TiO_2 and MgO contents (Supplementary Figures S3E, F), indicating that there was no accumulation of Fe-Ti oxide minerals, which is consistent with the mineral phases observed in photomicrographs (Figure 2). The no correlation between CaO/Al_2O_3 ratios and MgO contents indicate that the fractionation of clinopyroxene was negligible (Supplementary Figure S3A). No correlation between Al_2O_3 and MgO contents, weak Sr anomaly and absence of Eu anomaly, which means that no obvious fractionation of occurred during the magma evolution (Supplementary Figures S3, S6A, B). For P53, the change of $Mg^{\#}$ value, Cr and Ni as well as the positive correlation between $Mg^{\#}$ and Cr, $Mg^{\#}$ and Ni (Supplementary Figures S3G, H) indicate that they may have experienced the fractionation of olivine or clinopyroxene. The weak correlation between CaO/Al_2O_3 and MgO, SiO_2 and MgO as well as CaO and MgO contents (Supplementary Figures S3A–C) may be explained by weak fractional crystallization of clinopyroxene and olivine. However, La (20.6–29.7 ppm) and La/Sm (4.5–5.2) values for the P53 samples follow the expected evolutionary path of partial melting rather than fractional crystallization. In addition, the insignificant Sr anomaly and the absence of Eu anomaly indicate that fractional crystallization of plagioclase is minimal (Figures 6C,D). The weak negative correlation between MgO and TiO_2 (Supplementary Figure S3E) may indicate the fractional crystallization of Fe-Ti oxide minerals, but there is no correlation between MgO and FeO^T contents (Supplementary Figure S3F) as well as no Fe-Ti oxide minerals are observed in the microphotographs. Therefore, fractionation crystallization has a limited effect on geochemical composition of P53 and can be ignored for P02.

In conclusion, the influence of later alteration, crustal contamination and fractional crystallization on the composition of the studied rocks are basically negligible. Therefore, the composition of these rocks was mainly controlled by the mineralogical and geochemical composition of their sources. In addition, the P53 has undergone weak alteration and weak fractional crystallization, and immobile elements (such as REE, HFSE, etc.) can be used to discriminate the nature of the magma source.

6.1.2 Mantle source

Both groups of rocks (P02 and P53) belong to calc-alkaline series (Figure 5C), with similar geochemical and isotopic compositions (Figure 6), which indicate that they have similar source regions. They have low SiO_2 (45.34–49.95 wt% and 50.06–56.24 wt%) and high MgO (7.14–8.66 wt% and 2.73–9.62 wt%) contents (Table 1), indicating that they are formed by partial melting of an ultramafic mantle source. In general, the mantle sources of mafic magma beneath the collision orogenic belt may be variable and complex (Mo et al., 2003; Chung et al., 2005; Dai et al., 2015; Fang et al., 2019; Niu et al., 2021; Sun et al., 2022; Villaseca et al., 2022). The magma derived from the asthenosphere mantle is equivalent to the mid-ocean ridge basalt (MORB) or oceanic island basalt (OIB) on the compositions of major-trace elements, which are marked by not depleting of HFSEs (Hofmann, 1988; Zou et al., 2000). In comparison, the magma derived from lithospheric mantle wedge show typical arc affinity signatures, such as enrichment of LILEs and LREEs, and depletion of HFSEs (Zhao and Zhou, 2007; Li et al., 2017; Niu et al., 2021). The two groups of rocks show arc-like trace element distribution patterns, enriched in REE and LILE (such as incompatible elements: Cs, Rb, Ba, Th, etc.) and depleted in HFSE (such as Nb, Ta, etc.), indicating that they originate from lithospheric mantle, and Zr/Nb ratios are significantly higher than OIB and La/Nb ratios >1.5 also proved this (Supplementary Table S3; Sun and McDonough, 1989). On the other hand, high initial $^{87}Sr/^{86}Sr$ ratios (0.70473–0.70811, 0.70599–0.70685), negative to positive εNd(t) values (−2.7 to +0.3, −1.0 to +1.5), obvious differentiation of LREE and HREE (La_N/Yb_N: 5.52–13.67) and positive anomalies of Pb (Supplementary Figures S6A, B; Table S4), these indicate that the mantle source had the addition of crustal material. This is supported by the ratios of trace elements that have different geochemical characteristics but similar incompatibilities, and which cannot be fractionated during magmatic processes. For instance, the ratios of Nb/U, Th/La, Nb/La, Ce/Pb, and Th/Nb are significantly different from those of the depleted mantle (Sun and McDonough, 1989; Salters and Stracke, 2004). These indicate that the mantle source may have been metasomatized by subduction-related components (Campbell, 2002). In addition, the two-stage model age (T_{DM2} (Nd): 1.1–1.4 Ga; Supplementary Table S4) consistent with the protolith age of UHP metamorphic rocks indicates that the subcontinent lithospheric mantle is a reasonable source region, as evidenced by all samples falling into the enriched subcontinent lithospheric mantle beneath the NQOB (Figure 7).

In summary, the arc-like trace element characteristics and enriched Sr-Nd isotopic compositions in the two groups of rocks show that they were derived from the enriched subcontinent lithospheric mantle beneath the NQOB, which was reformed by subduction-related crustal materials.

6.1.3 Modification of the subcontinental lithospheric mantle

Oceanic and continental arc magmatism are considered to be a typical product of oceanic subduction, while oceanic and continental-type eclogites are considered to be a typical product of oceanic/continental subduction to subarc depths. Compared with HP/UHP metamorphic rocks, arc-like mafic rocks carry more information about lithospheric mantle. Generally, calc-alkaline rocks are produced in the island-arc setting during oceanic subduction, and its trace element composition is characterized by depletion of Nb and Ta, enrichment of LILEs (Rb, Ba, Th, U, K, Pb and La), such as P02 (Figure 6B). In addition, the P53 formed during continental subduction-collision and some mafic rocks of post-collision also show the properties of typical island-arc rocks (Figures 5D, 6D). Therefore, there are continuous arc-like magmatism during oceanic subduction, continental subduction-collision and post-collision in the NQOB, and the magma originated from the lithospheric mantle previously modified by the subduction system (Zhao et al., 2018; Zhou et al., 2021).

Slab subduction is regarded as a crucial mechanism for bringing crustal components into the mantle, and the interaction between the subducted components and the overlying mantle determines the geochemical composition of the mantle-derived magma above the subduction zone (Elliott, 2003; Zhao et al., 2015; Fang et al., 2019). The depleted mantle generally shows depleted LILE and LREE, and the low Sr-Nd isotopes, are enriched after the metasomatism of the crustal material (Workman et al., 2003; Salters and Stracke, 2004; Workman and Hart, 2005; Willbold and Stracke, 2010). Common post-collisional mafic igneous rocks at the Sulu-Dabie show arc-like trace element distribution patterns and significantly enriched Sr-Nd isotopic compositions (Zhao et al., 2013). Such compositions are interpreted to have resulted from the incorporation of continental crust-derived materials into their mantle sources. This is because felsic melts formed by subducting continental crust typically exhibit arc-like trace element distribution patterns and enriched radiogenic isotopes, and if these melts reacted with the mantle, the crustal characteristics would be transferred to the final mafic rocks (Zheng and Hermann, 2014). However, P02, P53 and post-collisional mafic rocks at the NQOB exhibit mainly arc-like trace element distribution patterns and slightly enriched/depleted radiogenic isotopic compositions (Figures 5, 6). These indicate that the crustal materials involved in the mafic rocks cannot be the subducted continental crust. In addition, post-collision mafic rocks with slab-derived fluid enrichment trends in the NQOB (Figure 8). On the other hand, the subducted continental crust is relatively dry, and it is difficult to release enough fluids to modify the mantle at the subarc depth, but the subducted oceanic crust can bring a large amount of water into the subarc depth, which is conducive to partial melting or dehydration of the overlying mantle (Zhao et al., 2013; Dai et al., 2015; Zheng et al., 2018). Therefore, the derivatives of the oceanic crust are reasonable crustal components to add to mantle sources of P02 and P53, such as basaltic oceanic crust-derived fluids or overlying sediment-derived melts.

Refractory minerals such as rutile and garnet remain stable at subarc depths, meaning that the released fluid is depleted in HFSE and HREE but enriched in LILE and LREE, as garnet is the major host of HREE and rutile is the major host of HFSE such as Nb, Ta, and Ti (Zheng et al., 2011). Such fluid would react with the mantle to generate metasomatic mantle domains, which may undergo partial melting to produce mafic melts with arc-like trace element distribution patterns and relatively depleted radiogenic isotopes (Schmidt and Poli, 2003; Zheng et al., 2019), which is consistent with trace element composition of P02 and P53 but not consistent with the Sr-Nd isotopic compositions. In addition, the SiO_2 contents of the two groups of rocks are 45.34–49.95 wt%, 50.06–56.24 wt%, respectively, with low Nb/U and TiO_2/Al_2O_3 ratios (Figure 8A), which are similar to oceanic arc basalts and continental arc basaltic andesites (Kelemen et al., 2003). These features are consistent with metamorphic dehydration/partial melting of the subducting oceanic

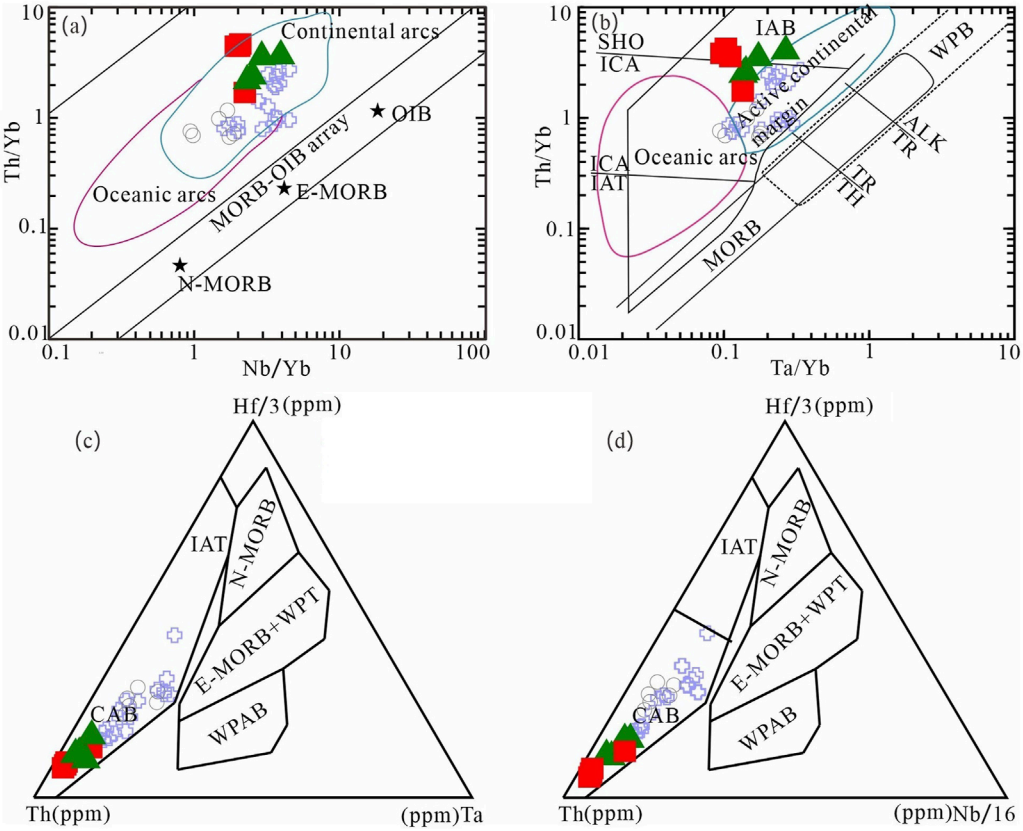

FIGURE 8
Plots of **(A)** Ce/Pb versus TiO2/Al2O3, **(B)** Th versus U/Th, **(C)** Ba/Th versus Th/Nb, and **(D)** Ba/Th versus (La/Yb) N for the Diorite (P53) and Gabbro (P02) of Yuka area (modified from Niu et al., 2021). Post-collisional intermediate/mafic rocks and gabbro from Zhao et al. (2018) and Zhou et al. (2021) (grey circle and light purple cross). The data for MORB and OIB are from Hofmann, (1988) and Sun and McDonough, (1989), respectively. The data for oceanic-arc basalts (OAB) and continental arc basaltic andesites (CAB) are from Kelemen et al. (2003). The data for island arc volcanic rocks are from Hawkesworth et al. (1997). The symbols are the same as in Figure 5.

crust in the rutile stability zone and oceanic crust-derived fluids are reasonable crustal components to add to mantle sources but do not exclude sediment-derived melts. The peridotite from Luliangshan of the NQOB also demonstrated the metasomatism of the mantle wedge by the fluids released by the subducting slab, and they have arc-like trace element compositions (Figure 6) and originated from the subcontinent lithosphere mantle (Xiong et al., 2015; Li et al., 2018). In addition, the ratios of U/Th, Th/Nb, Ba/Th and $(La/Yb)_N$ show insignificant enrichment trends, including fluid from oceanic crusts and melt from overlying sediments (Supplementary Table S3; Figure 8) (Hawkesworth et al., 1997; Elliott, 2003; Bebout, 2007; Zheng and Hermann, 2014; Zheng, 2019). Therefore, the enrichment of the subcontinent lithospheric mantle of the NQOB is mainly due to the contribution of fluids derived from subducted oceanic crust, with a small amount of melts derived from subducted sediments.

In summary, the NQOB has continuous arc-like magmatism of subcontinent lithospheric mantle generally metasomatized by fluids derived from the subducting oceanic crust. This metasomatic mantle source may not have undergone partial melting shortly after its early formation but was stored in the orogenic belt and became a potential source of subsequent mafic magmatism (Chen et al., 2016; Fang et al., 2019; Zheng et al., 2019).

6.2 Geodynamic process and multi-stage magmatism

Previous studies (Song et al., 2009a; Zhang et al., 2013; Song et al., 2014; Wu et al., 2019; Ren et al., 2019; Zhou et al., 2021; Zhou et al., 2021; Chen et al., 2022) have shown that the NQOB is a series of tectonic events that occurred from the early Paleozoic to the late Paleozoic, including oceanic subduction, continental subduction, collisional orogeny, slab exhumation, and post-orogenic extension. Several tectonic evolution models have been proposed to explain HP/UHP metamorphism and magmatism. For instance, Wu et al. (2019) divided the granites in the Wulan of the NQ into five stages based on age and geochemical characteristics: (1) 465–473 Ma, (2) 423–446 Ma, (3) 391–413 Ma, (4) 372–383 Ma and (5) 240–271 Ma, revealing tectonic evolution and geodynamic processes. However, mafic rocks originated from deep mantle and are more representative in revealing the nature of mantle and geodynamic processes, such as syn-collisional and post-collisional mafic rocks (Zhao et al., 2013; Dai et al., 2015; Fang et al., 2019; Niu et al., 2021).

6.2.1 Age of multi-stage mafic magmatism

Generally, the protolith ages of oceanic-type eclogites are usually consistent with the age of mafic rocks at a certain stage in the region, including the stage from the formation to the closure of the ocean basin (Zhang L. et al., 2008), the protolith of continental-type eclogites may represent the mafic rocks intruded during breakup of ancient supercontinent (Song et al., 2010; Zhang et al., 2009c; Zhang et al., 2011; Zhang G. B. et al., 2016), and mafic magmatism later than continental eclogite-facies metamorphism represent the mafic rocks intruded during exhumation or post-collision (Zhao et al., 2013; Zhao et al., 2017; Zhou et al., 2021). The ages of oceanic and continental-type eclogites in the NQOB are 465–445 Ma and 438–420 Ma, respectively, indicating that the continental crust subducted to the depth of the mantle after 440 Ma (Table 1). As shown in tables 1 and 2, there are multi-stages of mafic magmatism in the NQOB, and the ages range from Neoproterozoic to Late Paleozoic, which are responses to different tectonic activities.

Some scholars have reported Neoproterozoic mafic rocks of the continental rift tectonic setting in the NQOB, which have geochemical compositions similar to E-MORB, MORB, and WPB, and some have been interpreted as mid-ocean ridge ophiolites (Yang et al., 2004; Zhu et al., 2015). These mafic rocks suggest that the breakup of Rodinia supercontinent induced melting of the deep mantle and the ocean begins to develop. The ages of P02 gabbros are 471 Ma, have arc-like geochemical compositions (Figures 4, 6), and was formed in the island-arc setting on the active continental margin (Figure 9), indicating that the NQ was in a mature island-arc setting at this time. Previous studies on the chronology and tectonic setting of mafic rocks suggest that the subduction of the Paleozoic ocean should be earlier than 535 Ma (Zhu et al., 2014; Chen et al., 2020) and the closure of the ocean after 455 Ma (Zhu et al., 2010; Li et al., 2019) in the NQOB, these mafic rocks belong to the tholeiitic or calc-alkaline or potassium series (Figure 5) and FAB or N-MORB or OIB or arc-like trace element compositions. The ages of P53 diorites are 438 Ma, which is consistent with the age of UHP metamorphism of continental-type eclogites, representing the product during continental subduction-collision. In addition, intermediate-mafic rocks were discovered in the Wulan in the eastern part of the NQOB, with ages of 441–429 Ma, which was interpreted as syn-collision magmatic rocks (Niu et al., 2021). Therefore, the NQOB have intermediate-mafic magmatism in response to continental subduction-collision, they have arc-like or E-MORB geochemical compositions and belong to the calc-alkaline or tholeiite series. After deep subduction of continent and slab exhumation, the NQOB entered the post-orogenic tensional settings (Xiong et al., 2014; Zhao et al., 2018; Zhou et al., 2021). The post-collision intermediate-mafic rocks are reported in the Dulan, Luliangshan and Xitieshan of the NQOB, most of which have arc-like geochemical compositions and belong to the tholeiite or calc-alkaline series, the ages (393–360 Ma) are consistent with the post-collisional granites (Figures 5, 6).

In summary, mafic rocks are widely distributed in the NQOB, such as Yuka, Luliangshan, Xitieshan, Dulan, Wulan and Oulongbuluke microcontinent (Tables 1 and 2). These intermediate-mafic rocks have different geochemical compositions, the age ranges from 535 Ma to 360 Ma, belonging to the products of different evolutionary stages. According to the age, geochemical characteristics, tectonic background of mafic rocks and the age of UHP metamorphism, the Paleozoic mafic magmatism in the NQOB can be divided into three stages: (1) Oceanic subduction (535–455 Ma), (2) Continental initial collision: (441–429 Ma), and (3) post-collision: (393–360 Ma).

6.2.2 Geodynamic setting

Previous studies have shown that the NQOB experienced geodynamic processes such as slab subduction, back-arc extension, slab rollback, slab breakoff, lithosphere collapse and extension in Paleozoic, which were responded to HP/UHP metamorphism and granitic magmatism (Song et al., 2006; Song et al., 2014; Zhang L. et al., 2016; Zhao et al., 2018; Wu et al., 2019). Therefore, the geodynamic setting of the two groups of rocks in this paper may include: (1) slab retreat and associated back-arc extension (Shi et al., 2006; Zhu et al., 2010); (2) slab rollback during initial continental collision (Niu et al., 2021); (3) breakoff of subducting oceanic slab (Xiong et al., 2014; Zhou et al., 2021); and (4) orogenic lithospheric delamination, collapse and extension (Wang et al., 2014; Zhao et al., 2018; Zhou et al., 2021).

The coexistence of continental-type eclogites and oceanic-type eclogites in the NQOB indicates that both oceanic and continental crusts were subducted to the depths of the mantle and undergo ultra-high pressure metamorphism, and subsequently exposed due to slab breakoff (Zhang G. B. et al., 2008; Chen et al., 2009; Song et al., 2014; Zhang G. B. et al., 2016). Slab breakoff can lead to the asthenosphere rising, bringing a large amount of heat to induce partial melting of the lithospheric mantle (Huw Davies and von Blanckenburg, 1995). However, the age of UHP metamorphism of continental-type eclogites is 438-420Ma (Table 1) and the study of granite in Wulan indicates that the slab breakoff and exhumation of continental crust occurred between 420 Ma and 397 Ma (Wu et al., 2019), which is inconsistent with the magmatic crystallization ages of P02 and P53 (471 and 438 Ma). After the exhumation of subduction slab, the NQOB experienced lithosphere delamination, collapse and extension (390–360 Ma; Song et al., 2014; Wang et al., 2014; Wu C. et al., 2014; Zhao et al., 2018; Zhou et al., 2021). Therefore, slab breakoff and lithosphere delamination, collapse and extension cannot be used to explain the geodynamic background of P02 and P53 magmatism.

Arc magmatism is common above oceanic subduction zone, and if the overlying lithosphere is relatively thin and hot or thermal convection during oceanic subduction, the metasomatic mantle domain is prone to partial melting. The arc magmatism related with subduction in the NQOB ranges from 535 to 446 Ma and the arc-backarc system terminated at 446 Ma (Tables 1, 2), which is consistent with the age of P02 magmatism (471Ma). On the other hand, P02 gabbros emplaced into the Tanjianshan Group in the island-arc setting, belong to the calc-alkaline series, and have arc-like geochemical compositions (Figures 5, 6). In addition, P02 gabbros show obvious affinity of island-arc tectonic environment (Figure 9) and classical island-arc rocks (Figure 5). Thus, these indicate that the geodynamic setting of P02 magmatism can be explained by retreat of the subducted oceanic slab and associated arc-backarc extension.

Slab rollback is an effective mechanism for the separation of the subduction slab and the overlying mantle wedge. At the beginning of the initial continental collision, the subducted oceanic slab occur rollback and steepening, which would cause tectonic extension, flux of heat into the overlying mantle and heating the previous metasomatic mantle, thereby inducing magmatism (Ding et al.,

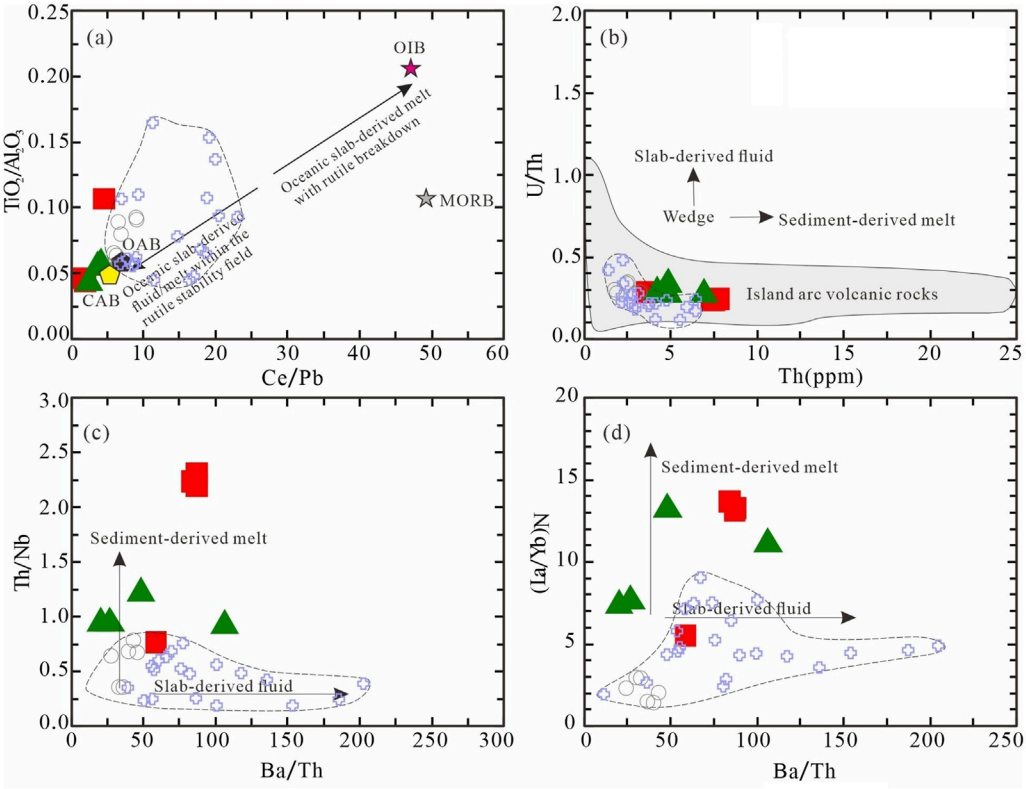

FIGURE 9
Tectonic setting discrimination diagrams for the Diorite (P53) and Gabbro (P02) of Yuka terrane. Post-collisional intermediate/mafic rocks and gabbro from Zhao et al., 2018; Zhou et al. (2021) (grey circle and light purple cross). **(A)** Th/Yb vs Nb/Yb diagram (after Pearce, 2008). **(B)** Ta/Yb versus Th/Yb (after Pearce, 1982). **(C)** Th-Hf/3-Ta diagram (after Wood, 1980). **(D)** Th-Hf/3-Nb/16 diagram (after Wood, 1980). ALK, Alkalic basalt; CAB, Calc-alkaline basalt; IAB, Island arc basalt; IAT, Island arc tholeiite; ICA, Island calc-alkaline; MORB, Mid- Ocean ridge basalt; OIB, Ocean Island basalt; SHO, Shoshonite; WPAB, Within-plate alkalic basalt; WPT, Within-plate tholeiite; TH, Tholeiitic basalt; TR, Transitional basalt. The symbols are the same as in Figure 5.

2005; Fang et al., 2019; Niu et al., 2021). The magmatic crystallization ages of P53 (438 Ma) is younger than that of subduction-related arc magmas (Tables 1 and 2, 535–446 Ma), slightly earlier than the age of UHP metamorphism of continental-type eclogites (438–420 Ma). This time relationship indicates that P53 magmatism occurred during the tectonic transition from oceanic subduction to continental subduction/collision. Therefore, the P53 magmatism is a response to the subduction-collision between the Qaidam block and the Qilian block, and rollback of the previously subducted oceanic slab is reasonable geodynamic setting of this magmatism. The partial melting of the ascending asthenosphere or enriched subcontinental lithospheric mantle produced E-MORB-type or arc-like magmatic rocks in the NQOB, the ages of magmatic crystallization ranges from 441 to 428 Ma, which also evidenced this process (Niu et al., 2021).

Taken together, the P02 and P53 magmatisms reveal a geodynamic transformation from the retreat of the subducting oceanic slab and the associated back-arc extension to slab rollback. The multistage mafic magmatism and UHP metamorphism indicate four distinct stages of geodynamic processes in the NQOB (Figure 10): (1) slab retreat and back-arc extension (535–445 Ma), (2) slab rollback (440–430 Ma), (3) slab breakoff (from 420 Ma onward), and (4) orogenic lithospheric delamination, collapse, and extension (390–360 Ma).

6.3 Implications for tectonic transition

The NQOB experienced a series of tectonic evolution in Paleozoic, such as oceanic subduction, continental subduction-collision and post-orogenic extension (Zhang et al., 2013; Song et al., 2014; Song et al., 2015; Zhang L. et al., 2016; Zhang C. et al., 2017; Zhao et al., 2018; Ren et al., 2019). The magmatism and metamorphism associated with these tectonic events are quite extensive, such as eclogite facies metamorphism and multi-stage mafic magmatism (Tables 1 and 2). Based on the previous discussion, we summarize a model of tectonic transition.

Ocean subduction (535–445 Ma) - slab retreat and associated back-arc extension: The South Qilian Ocean subducted beneath the Qilian Block; the overlying subcontinent lithospheric mantle was metasomatized by fluids originating from the oceanic crust at subarc depths. Partial melting of metasomatized mantle domains produced arc magmatism related to slab subduction (e.g., P02), while some metasomatized mantle domains were preserved in

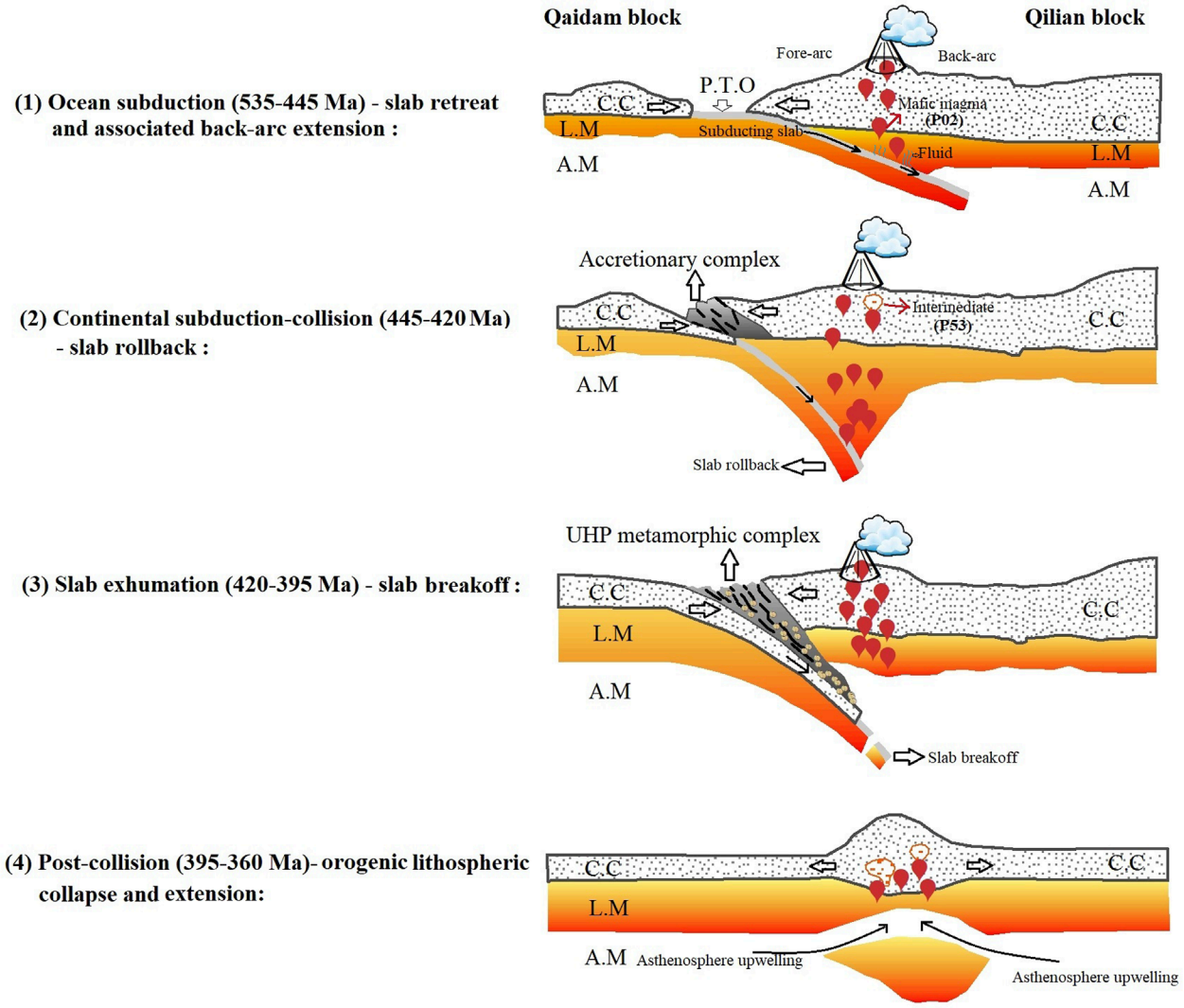

FIGURE 10
A conceptual geodynamic model of the NQOB: C.C., Continental Crust; L.M., Lithospheric Mantle; P.T.O., Proto-Tethyan Ocean; A.M., Asthenospheric Mantle.

the orogenic lithosphere, serving as potential sources for later arc magmatism (e.g., P53). During this period, the NQOB also existed mafic magmatism originating from the asthenospheric mantle and depleted mantle (Table 2, 535–455 Ma). Furthermore, the subducted oceanic crust underwent UHP metamorphism in the deep mantle, resulting in oceanic-type eclogites with the age of 465–455 Ma (Table 1).

Continental subduction-collision (445–420 Ma) - slab rollback: The initial collision of the Qaidam and Qilian blocks led to the rollback of the subducting slab, and the asthenospheric mantle upwelling and lateral flow induced the partial melting of the previous metasomatic mantle domain to produce arc-like rocks (e.g., P53). The syncollisional intermediate-mafic magmatic rocks with the age of 441–429 Ma in the NQOB, which also indicates the geodynamic process of slab rollback (Niu et al., 2021). A similar example was reported in the Dabie-Sulu orogenic belt, the slab rollback caused partial melting of the metasomatic mantle to generate mafic magma during the initial continental collision (Fang et al., 2019). Furthermore, continental crust of the Qaidam block was dragged by the subducting relatively dense oceanic lithosphere to mantle depths (>100 km), which resulted in UHP metamorphism and generated continental-type eclogites with the age of 438–420 Ma (Table 1).

Slab exhumation (420–395 Ma) - slab breakoff: This stage lacked mafic magmatism and only pyroxenite dykes were reported in Luliangshan of the NQOB (Xiong et al., 2014). The study of eclogites and granites indicates that the exhumation of continental crust occurred between 420 Ma and 397 Ma (e.g., Mattinson et al., 2006; Zhang et al., 2011; ZhangG. B. et al., 2016; Chen et al., 2022).

Post-collision (395–360 Ma)-orogenic lithospheric collapse and extension: The age of continental-type eclogites and granites indicates that the age of slab breakoff and slab exhumation is after 420 Ma, and then entered the post-collisional orogenic setting (Table 1) (Wu et al., 2019). The collapse and extension of the orogenic lithospheric led to the upwelling of the asthenosphere,

which induced partial melting of the metasomatic mantle domain, resulting in the post-collisional arc-like mafic magmatism with the age of 393–360 Ma (Table 2).

7 Conclusion

A comprehensive study of thin-section analysis, zircon U-Pb dating, whole-rock major-trace element analysis, and whole-rock Sr-Nd isotopic analysis of diorite (P53) and gabbro (P02) rocks from the Yuka terrane in the North Qaidam Orogenic Belt (NQOB) led to the following conclusions.

1. In the Yuka terrane, gabbro (P02) originated during the oceanic subduction stage at 471 Ma, and diorite (P53) formed during the continental subduction-collision stage at 438 Ma.
2. As a result of partial melting of the enriched subcontinental lithospheric mantle, gabbro (P02) and diorite (P53) exhibit moderate ($^{87}Sr/^{86}Sr$)i values (0.70473–0.70811 and 0.70599 to 0.70685, respectively) and positive to negative εNd(t) values (−2.7 to +0.3 and −1.0 to +1.5, respectively).
3. Both gabbro and diorite exhibit arc-like trace element compositions, indicating derivation from the subcontinental lithospheric mantle, metasomatized by fluids from previously subducted oceanic crust at subarc depths within the rutile stability zone.
4. Paleozoic mafic magmatism in the NQOB can be divided into three stages: (1) Oceanic subduction (535–455 Ma), (2) Continental initial collision (441–429 Ma), and (3) post-collision (393–360 Ma).
5. The NQOB also underwent four stages of geodynamic processes: (1) 535–445 Ma: Oceanic subduction, slab retreat, and back-arc extension; (2) 445–420 Ma: Continental subduction and collision, followed by slab rollback; (3) 420–395 Ma: Exhumation of oceanic and continental crust, and slab breakoff; (4) 395–360 Ma: Post-collisional orogenic collapse and lithospheric extension.

Data availability statement

The original contributions presented in the study are included in the article/Supplementary Material, further inquiries can be directed to the corresponding author.

Author contributions

YL: Conceptualization, Data curation, Funding acquisition, Investigation, Methodology, Software, Supervision, Validation, Visualization, Writing–original draft. CY: Conceptualization, Data curation, Funding acquisition, Investigation, Methodology, Software, Validation, Visualization, Writing–original draft. SC: Conceptualization, Data curation, Funding acquisition, Investigation, Methodology, Software, Validation, Visualization, Writing–original draft. SS: Conceptualization, Data curation, Funding acquisition, Investigation, Methodology, Software, Validation, Visualization, Writing–original draft. SL: Conceptualization, Data curation, Formal Analysis, Investigation, Methodology, Software, Validation, Visualization, Writing–original draft. JK: Writing–review and editing.

Funding

The author(s) declare that financial support was received for the research, authorship, and/or publication of this article. This research was financially supported by the Qinghai Science and Technology Planning Project (2021-ZJ-741).

Acknowledgments

We thank all those who helped us complete this research work. Special thanks to Editor Prof. Yong Wang and the reviewers for their critical comments and constructive suggestions, which significantly improved the quality of the paper. We also thank the laboratories for providing the opportunity to conduct analyses, and Asma from the China University of Geosciences, Wuhan, for her review and proofreading.

Conflict of interest

Authors YL, SC, SS, and SL were employed by Tibet Xianglong Copper Industry Limited Company.

The remaining authors declare that the research was conducted in the absence of any commercial or financial relationships that could be construed as a potential conflict of interest.

Generative AI statement

The author(s) declare that no Generative AI was used in the creation of this manuscript.

Publisher's note

All claims expressed in this article are solely those of the authors and do not necessarily represent those of their affiliated organizations, or those of the publisher, the editors and the reviewers. Any product that may be evaluated in this article, or claim that may be made by its manufacturer, is not guaranteed or endorsed by the publisher.

Supplementary material

The Supplementary Material for this article can be found online at: https://www.frontiersin.org/articles/10.3389/feart.2025.1545127/full#supplementary-material

References

Bebout, G. E. (2007). Metamorphic chemical geodynamics of subduction zones. *Earth Planet. Sci. Lett.* 260 (3), 373–393. doi:10.1016/j.epsl.2007.05.050

Bouvier, A., Vervoort, J. D., and Patchett, P. J. (2008). The Lu-Hf and Sm-Nd isotopic composition of CHUR: constraints from unequilibrated chondrites and implications for the bulk composition of terrestrial planets. *Earth Planet. Sci. Lett.* 273 (1), 48–57. doi:10.1016/j.epsl.2008.06.010

Boynton, W. V., Henderson, P., Henderson, P., and Hendersons, P. (1984). "Chapter 3 - cosmochemistry of the rare earth elements: meteorite studies," in *Developments in geochemistry*. Elsevier, 63–114.

Cai, P., Chen, X., Majka, J., Klonowska, I., Jeanneret, P., Xu, R., et al. (2021). Two stages of crust-mantle interaction during oceanic subduction to continental collision: Insights from mafic-ultramafic complexes in the North Qaidam orogen. *Gondwana Res.* 89, 247–264. doi:10.1016/j.gr.2020.08.018

Campbell, I. H. (2002). Implications of Nb/U, Th/U and Sm/Nd in plume magmas for the relationship between continental and oceanic crust formation and the development of the depleted mantle. *Geochimica Cosmochimica Acta* 66 (9), 1651–1661. doi:10.1016/s0016-7037(01)00856-0

Chen, D., Liu, L., Sun, Y., Sun, W. D., Zhu, X. H., Liu, X. M., et al. (2012). Felsic veins within UHP eclogite at xitieshan in North Qaidam, NW China: partial melting during exhumation. *Lithos* 136 (SI), 187–200. doi:10.1016/j.lithos.2011.11.006

Chen, D., Sun, Y., Liu, L., Zhang, A., and Lin, C. (2007). *In situ* LA-ICP-MS zircon U-Pb age of ultrahigh-pressure eclogites in the Yukahe area, northern Qaidam Basin. *Earth Sci.* 50 (S2), 322–330. doi:10.1007/s11430-007-6001-6

Chen, D., Zhu, X., Ren, Y., and Tuo, Y. (2020). Early Paleozoic ocean in the North Qaidam: constraints from kaipinggou ophiolite. *Acta Geol. Sin.* 941 (SI), 6. doi:10.1111/1755-6724.14428

Chen, D. L., Liu, L., Sun, Y., and Liou, J. G. (2009). Geochemistry and zircon U-Pb dating and its implications of the Yukahe HP/UHP terrane, the North Qaidam, NW China. *J. Asian Earth Sci.* 35 (3-4SI), 259–272. doi:10.1016/j.jseaes.2008.12.001

Chen, D. L., Sun, Y., Liu, L., Zhang, A. D., Luo, J. H., and Wang, Y. (2005). Metamorphic evolution of the Yuka eclogite in the North Qaidam, NW China: evidences from the compositional zonation of garnet and reaction texture in the rock. *Acta Petrol. Sin.* 21(4):1039–1048.

Chen, L., Ma, C., Zhang, J., Mason, R., and Zhang, C. (2011). Mafic dykes derived from Early Cretaceous depleted mantle beneath the Dabie orogenic belt: implications for changing lithosphere mantle beneath Eastern China. *Geol. J.* 46 (4), 333–343. doi:10.1002/gj.1273

Chen, L., and Zhao, Z. (2017). Origin of continental arc andesites: the composition of source rocks is the key. *J. Asian Earth Sci.*, 145: 217–232. doi:10.1016/j.jseaes.2017.04.012

Chen, L., Zheng, Y., and Zhao, Z. (2016). Geochemical constraints on the origin of late mesozoic andesites from the ningwu basin in the middle-lower yangtze valley, South China. *Lithos* 254-255, 94–117. doi:10.1016/j.lithos.2016.03.012

Chen, N., Liao, F., Wang, L., Santosh, M., Sun, M., Wang, Q., et al. (2013). Late paleoproterozoic multiple metamorphic events in the quanji massif: links with Tarim and north China cratons and implications for assembly of the columbia supercontinent. *Precambrian Res.* 228, 102–116. doi:10.1016/j.precamres.2013.01.013

Chen, X., Jiang, S., Palmer, M. R., Schertl, H. P., Cambeses, A., Hernández-Uribe, D., et al. (2023). Tourmaline chemistry, boron, and strontium isotope systematics trace multiple melt–fluid–rock interaction stages in deeply subducted continental crust. *Geoch. Cosm. Act.* 340, 120–140. doi:10.1016/j.gca.2022.11.019

Chen, X., Schertl, H., Cambeses, A., Gu, P., Xu, R., Zheng, Y., et al. (2019). From magmatic generation to UHP metamorphic overprint and subsequent exhumation: a rapid cycle of plate movement recorded by the supra-subduction zone ophiolite from the North Qaidam orogen. *Lithos* 350-351, 105238. doi:10.1016/j.lithos.2019.105238

Chen, X., Schertl, H. P., Chopin, C., Lin, C., Lin, H., Li, H., et al. (2024). From divergent to convergent plate boundary: a ca. 200 Ma Wilson cycle recorded by ultrahigh-pressure eclogites in the Dora-Maira Massif, Western Alps. *Bulletin* 136 (5–6), 2178–2194. doi:10.1130/B37045.1

Chen, X., Schertl, H. P., Cambeses, A., Hart, E., Lin, C., Xu, R., et al. (2022a). Cyclicity of multistage anatexis of deeply subducted continental crust during the North Qaidam orogeny: Tracing the source, timescale, and evolution of pulsed melts. *Am. J. Sci.* 322 (2), 225–279. doi:10.2475/02.2022.05

Chen, X., Schertl, H. P., Hart, E., Majka, J., Cambeses, A., Hernández-Uribe, D., et al. (2022b). Mobilization and fractionation of Ti-Nb-Ta during exhumation of deeply subducted continental crust. *Geoch. Cosm. Act.* 319, 271–295. doi:10.1016/j.gca.2021.11.024

Chen, X., Schertl, H. P., Khan, J., Cai, P., Lian, D., Wang, J., et al. (2025). Scandium mineralization during ultramafic-mafic magmatism in the subduction zone. *Chem. Geol.* 673, 122556. doi:10.1016/j.chemgeo.2024.122556

Chen, X., Xu, R., Zheng, Y., and Cai, P. (2018). Petrology and geochemistry of high niobium eclogite in the North Qaidam orogen, Western China: implications for an eclogite facies metamorphosed island arc slice. *J. Asian Earth Sci.* 164, 380–397. doi:10.1016/j.jseaes.2018.07.003

Chen, X., Xu, R., Zheng, Y., Gao, S., Cai, P., Yu, J., et al. (2019). The geodynamic setting of Dulan eclogite-type rutile deposits in the North Qaidam orogen, western China. *Ore Geol. Rev.* 110, 102936. doi:10.1016/j.oregeorev.2019.102936

Chen, X., Zheng, Y., Xu, R., Gu, P., Yu, J., Bai, J., et al. (2020). Subduction channel fluid-rock interaction: indications from rutile-quartz veins within eclogite from the Yuka terrane, North Qaidam orogen. *Geosci. Front.* 11 (2), 635–650. doi:10.1016/j.gsf.2019.07.009

Chung, S., Chu, M., Zhang, Y., Xie, Y., Lo, C. H., Lee, T. Y., et al. (2005). Tibetan tectonic evolution inferred from spatial and temporal variations in post-collisional magmatism. *Earth-Science Rev.* 68 (3-4), 173–196. doi:10.1016/j.earscirev.2004.05.001

Coltorti, M., Bonadiman, C., Faccini, B., Ntaflos, T., and Siena, F. (2007). Slab melt and intraplate metasomatism in Kapfenstein mantle xenoliths (Styrian Basin, Austria). *Lithos* 94 (1), 66–89. doi:10.1016/j.lithos.2006.07.003

Cook, Y. A., Sanislav, I. V., Hammerli, J., Blenkinsop, T. G., and Dirks, P. H. G. M. (2016). A primitive mantle source for the Neoarchean mafic rocks from the Tanzania Craton. *Geosci. Front.* 7 (6), 911–926. doi:10.1016/j.gsf.2015.11.008

Corfu, F., Hanchar, J. M., Hoskin, P. W. O., and Kinny, P. (2003). Atlas of zircon textures. *Rev. Mineralogy Geochem.* 53 (1), 469–500. doi:10.2113/0530469

Dai, L., Zhao, Z., and Zheng, Y. (2015). Tectonic development from oceanic subduction to continental collision: geochemical evidence from post-collisional mafic rocks in the Hong'an-Dabie orogens. *Gondwana Res.* 27 (3), 1236–1254. doi:10.1016/j.gr.2013.12.005

Ding, L., Kapp, P., and Wan, X. (2005). Paleocene-Eocene record of ophiolite obduction and initial India-Asia collision, South central Tibet. *Tectonics* 24, TC3001. doi:10.1029/2004tc001729

Elliott, T. (2003). Tracers of the slab. *Geophys. Monograph-American Geophys. Union* 138, 23–46. doi:10.1029/138GM03

Ernst, W. G., and Liou, J. G. (1999). Overview of UHP metamorphism and tectonics in well-studied collisional orogens. *Int. Geol. Rev.* 41 (6), 477–493. doi:10.1080/00206819909465153

Fang, W., Dai, L., Zheng, Y., Zhao, Z., and Ma, L. (2019). Tectonic transition from oceanic subduction to continental collision: new geochemical evidence from Early-Middle Triassic mafic igneous rocks in southern Liaodong Peninsula, east-central China. *GSA Bull.* 132 (7-8), 1469–1488. doi:10.1130/b35278.1

Fu, J., Liang, X., Wang, C., Zhou, Y., Jiang, Y., and Dong, C. (2017). The Xitieshan volcanic sediment-hosted massive sulfide deposit, North Qaidam, China: Geology, structural deformation, and geochronology. *Ore Geol. Rev.* 80, 923–946. doi:10.1016/j.oregeorev.2016.08.027

Gao, X., Yu, S., Peng, Y., Lv, P., Wang, M., Liu, Y., et al. (2021). Insights into OIB-like magmatism contemporaneous with oceanic subduction: petrogenetic constraints on the Kendelong metagabbro in the North Qaidam. *Lithos* 392, 106130. doi:10.1016/j.lithos.2021.106130

Guo, J., Li, Y., Palin, R. M., Zhang, J., and Yu, S. (2023). Evolution and modification of lithospheric mantle within deeply continental subduction zone: insights from two contrasting orogenic garnet peridotites in South Altun–North Qaidam belt. *Lithos* 450-451, 107185. doi:10.1016/j.lithos.2023.107185

Hansen, J., Skjerlie, K. P., Pedersen, R. B., and De La Rosa, J. (2002). Crustal melting in the lower parts of island arcs: an example from the Bremanger Granitoid Complex, west Norwegian Caledonides. *Contributions Mineralogy Petrology* 143, 316–335. doi:10.1007/s00410-001-0342-5

Hans Wedepohl, K. (1995). The composition of the continental crust. *Geochimica Cosmochimica Acta* 59 (7), 1217–1232. doi:10.1016/0016-7037(95)00038-2

Hawkesworth, C., Turner, S., McDermott, F., Peate, D., and Calsteren, P. (1997). U-Th isotopes in arc magmas: implications for element transfer from the subducted crust. *Science* 276, 551–555. doi:10.1126/science.276.5312.551

Herzberg, C. (2006). Petrology and thermal structure of the Hawaiian plume from Mauna Kea volcano. *Nature* 444 (7119), 605–609. doi:10.1038/nature05254

Hofmann, A. W. (1988). Chemical differentiation of the Earth: the relationship between mantle, continental crust, and oceanic crust. *Earth Planet. Sci. Lett.* 90 (3), 297–314. doi:10.1016/0012-821x(88)90132-x

Hofmann, A. W. (1997). Mantle geochemistry: the message from oceanic volcanism. *Nat. Lond.* 385 (6613), 219–229. doi:10.1038/385219a0

Hoskin, P., and Schaltegger, U. (2003). The composition of zircon and igneous and metamorphic petrogenesis. *Rev. Mineralogy Geochem.* 53, 27–62. doi:10.2113/0530027

Huw Davies, J., and von Blanckenburg, F. (1995). Slab breakoff: a model of lithosphere detachment and its test in the magmatism and deformation of collisional orogens. *Earth Planet. Sci. Lett.* 129 (1), 85–102. doi:10.1016/0012-821x(94)00237-s

Irvine, T. N., and Baragar, W. R. A. F. (1971). A guide to the chemical classification of the common volcanic rocks. *Can. J. earth Sci.* 8 (5), 523–548. doi:10.1139/e71-055

Kelemen, P., Hanghøj, K., and Greene, A. (2003). One view of the geochemistry of subduction-related magmatic arcs, with an emphasis on primitive andesite and lower crust. *Treatise Geochem.* 3, 593–659. doi:10.1016/B0-08-043751-6/03035-8

Khan, J., Yao, H., Zhao, J., Li, Q., Xiang, W., Jiang, J., et al. (2023). Petrogenesis and tectonic implications of the tertiary choke shield basalt and continental flood basalt from the central Ethiopian plateau. *J. Earth Sci.* 34 (1), 86–100. doi:10.1007/s12583-022-1729-7

Khan, J., Yao, H.-Z., Zhao, J.-H., Tahir, A., Chen, K.-X., Wang, J.-X., et al. (2024). Geochronology, geochemistry, and tectonic setting of the Neoproterozoic magmatic rocks in Pan-African basement, West Ethiopia. *Ore Geol. Rev.* 164, 105858. doi:10.1016/j.oregeorev.2023.105858

Le Maitre, R. W. V., Bateman, P., and Dudek, A. V. (1989). *A classification of igneous rocks and glossary of terms: recommendations of the international union of geological sciences, subcommission on the systematics of igneous rocks*. Oxford: Blackwell.

Li, C., Li, X., Li, Q., Guo, J. H., and Yang, Y. H. (2012). Rapid and precise determination of Sr and Nd isotopic ratios in geological samples from the same filament loading by thermal ionization mass spectrometry employing a single-step separation scheme. *Anal. Chim. Acta* 727, 54–60. doi:10.1016/j.aca.2012.03.040

Li, F., Wu, Z. L., Li, B. Z., and Wang, L. F. (2006). Revision of the tanjianshan group on the northern margin of the Qaidam basin. *Northwest. Geol.* 39 (3), 83–90. doi:10.12401/j.nwg.20060312

Li, H. R., Sun, F. Y., Li, L., and Yan, J. M. (2019). The Hudesheng mafic-ultramafic intrusions in the Oulongbuluke Block, Qinghai Province, NW China: chronology, geochemistry, isotopic systematics and tectonic implications. *Geol. Mag.* 156 (9), 1527–1546. doi:10.1017/s0016756818000778

Li, Y., Brouwer, F. M., Xiao, W., Wang, K. L., Lee, Y. H., Luo, B., et al. (2017). Subduction-related metasomatic mantle source in the eastern central asian orogenic belt: evidence from amphibolites in the xilingol complex, inner Mongolia, China. *Gondwana Res.* 43, 193–212. doi:10.1016/j.gr.2015.11.015

Li, Y., Zhang, J., Mostofa, K. M. G., Wang, Y., Yu, S., Cai, Z., et al. (2018). Petrogenesis of carbonatites in the Luliangshan region, North Qaidam, northern Tibet, China: evidence for recycling of sedimentary carbonate and mantle metasomatism within a subduction zone. *Lithos* 322, 148–165. doi:10.1016/j.lithos.2018.10.010

Liang, X., Fu, J., Wang, C., Jiang, Y., Zhou, Y., Yang, Y., et al. (2014). Redefinition and formation age of the tanjianshan group in xitieshan region, Qinghai. *Acta Geol. Sin.* 88 (2), 394–409. doi:10.1111/1755-6724.12204

Liao, F. X., Chen, N. S., Santosh, M., Wang, Q. Y., Gong, S. L., He, C., et al. (2018). Paleoproterozoic Nb-enriched meta-gabbros in the quanji massif, NW China: implications for assembly of the columbia supercontinent. *Geosci. Front.* 9 (2), 577–590. doi:10.1016/j.gsf.2017.05.007

Liew, T. C., and Hofmann, A. W. (1988). Precambrian crustal components, plutonic associations, plate environment of the Hercynian Fold Belt of central Europe: indications from a Nd and Sr isotopic study. *Contributions Mineralogy Petrology* 98 (2), 129–138. doi:10.1007/bf00402106

Lin, J., Liu, Y., Yang, Y., and Hu, Z. (2016). Calibration and correction of LA-ICP-MS and LA-MC-ICP-MS analyses for element contents and isotopic ratios. *Solid Earth Sci.* 1 (1), 5–27. doi:10.1016/j.sesci.2016.04.002

Liu, Y., Gao, S., Hu, Z., Gao, C., Zong, K., and Wang, D. (2010). Continental and oceanic crust recycling-induced MeltPeridotite interactions in the trans-north China orogen: UPb dating, Hf isotopes and trace elements in zircons from mantle xenoliths. *J. Petrology* 51 (1-2), 537–571. doi:10.1093/petrology/egp082

Liu, Y., Hu, Z., Gao, S., Günther, D., Xu, J., Gao, C., et al. (2008a). *In situ* analysis of major and trace elements of anhydrous minerals by LA-ICP-MS without applying an internal standard. *Chem. Geol.* 257 (1), 34–43. doi:10.1016/j.chemgeo.2008.08.004

Liu, Y., Zong, K., Kelemen, P. B., and Gao, S. (2008b). Geochemistry and magmatic history of eclogites and ultramafic rocks from the Chinese continental scientific drill hole: subduction and ultrahigh-pressure metamorphism of lower crustal cumulates. *Chem. Geol.* 247 (1), 133–153. doi:10.1016/j.chemgeo.2007.10.016

Lu, S., Li, H., Zhang, C., and Niu, G. (2008). Geological and geochronological evidence for the Precambrian evolution of the Tarim Craton and surrounding continental fragments. *Precambrian Res.* 160 (1), 94–107. doi:10.1016/j.precamres.2007.04.025

Lu, S. N., Wang, H. C., Li, H., Yuan, G. B., Xin, H. T., and Zheng, J. K. (2002). Redefinition of the "Dakendaban Group" on the northern margin of the Qaidam basin. *Geol. Bull. China* 21 (1), 19–23.

Lu, Z. L., Zhang, J. X., Mao, X. H., GuiSheng, Z., Xia, T., and YaWei, W. (2020). Ordovician adakite-Nb-enriched basalt suite in the eastern North Qaidam Mountains: implications for oceanic subduction and crustal accretion prior to deep continental subduction. *Acta Petrol. Sin.* 36 (10), 2995–3017. doi:10.18654/1000-0569/2020.10.05

Ludwig, K. R. (2003). *User's manual for Isoplot 3.00 - a geochronological toolkit for microsoft excel*. California, Berkeley: Berkeley Geochronology Center, 39.

Mattinson, C. G., Wooden, J. L., Liou, J. G., Bird, D. K., and Wu, C. L. (2006). Age and duration of eclogite-facies metamorphism, North Qaidam HP/UHP terrane, Western China. *Geochimica Cosmochimica Acta* 70 (18), A401. doi:10.1016/j.gca.2006.06.809

McCarthy, A., Chelle-Michou, C., Müntener, O., Arculus, R., and Blundy, J. (2018). Subduction initiation without magmatism: the case of the missing Alpine magmatic arc. *Geology* 46 (12), 1059–1062. doi:10.1130/g45366.1

Mo, X., Niu, Y., Dong, G., Zhao, Z., Hou, Z., Zhou, S., et al. (2008). Contribution of syncollisional felsic magmatism to continental crust growth: a case study of the Paleogene Linzizong volcanic Succession in southern Tibet. *Chem. Geol.* 250 (1-4), 49–67. doi:10.1016/j.chemgeo.2008.02.003

Mo, X. X., Zhao, Z., and Deng, J. (2003). Response of volcanism to the India-Asia collision. *Earth Sci. Front.* 10, 135–148.

Niu, M. L., Cai, Q. R., Li, X. C., Yakymchuk, C., Wu, Q., Yuan, X., et al. (2021). Early Paleozoic tectonic transition from oceanic to continental subduction in the North Qaidam tectonic belt: constraints from geochronology and geochemistry of syncollisional magmatic rocks. *Gondwana Res.* 91, 58–80. doi:10.1016/j.gr.2020.10.018

Niu, Y., Zhao, Z., Zhu, D., and Mo, X. (2013). Continental collision zones are primary sites for net continental crust growth — a testable hypothesis. *Earth-Science Rev.* 127, 96–110. doi:10.1016/j.earscirev.2013.09.004

Pearce, J. A. (1982). "Trace element characteristics of lavas from destructive plate boundaries," in *Andesites: Orogenic Andesites and Related Rocks*. Editor R. S. Thorpe (Chichester: John Wiley & Sons), 525–548.

Pearce, J. A. (2008). Geochemical fingerprinting of oceanic basalts with applications to ophiolite classification and the search for Archean oceanic crust. *Lithos* 100 (1), 14–48. doi:10.1016/j.lithos.2007.06.016

Plank, T., and Langmuir, C. H., (1998). The chemical composition of subducting sediment and its consequences for the crust and mantle. *Chem. Geol.*, 145 (3): 325–394. doi:10.1016/s0009-2541(97)00150-2

Ren, Y., Chen, D., Kelsey, D. E., Gong, X., and Liu, L. (2017). Petrology and Geochemistry of the lawsonite (pseudomorph)-bearing eclogite in Yuka terrane, North Qaidam UHPM belt: an eclogite facies metamorphosed oceanic slice. *Gondwana Res.* 42, 220–242. doi:10.1016/j.gr.2016.10.011

Ren, Y., Chen, D., Zhu, X., Ren, Z., and Gong, X. (2019). Two orogenic cycles recorded by eclogites in the Yuka-Luofengpo terrane: implications for the Mesoproterozoic to early Paleozoic tectonic evolution of the North Qaidam orogenic belt, NW China. *Precambrian Res.* 333, 105449. doi:10.1016/j.precamres.2019.105449

Roden, M. F., and Murthy, V. R. (1985). Mantle metasomatism. *Annu. Rev. Earth Planet. Sci.* 13 (1), 269–296. doi:10.1146/annurev.earth.13.1.269

Rudnick, R., and Gao, S. (2003). Composition of the continental crust. *Treatise Geochem.* 3, 1–64. doi:10.1016/b0-08-043751-6/03016-4

Rudnick, R. L., Gao, S., Ling, W., Liu, Y., and McDonough, W. F. (2004). Petrology and geochemistry of spinel peridotite xenoliths from Hannuoba and Qixia, North China craton. *Lithos* 77 (1), 609–637. doi:10.1016/j.lithos.2004.03.033

Rumble, D., Liou, J., and Jahn, B. (2003). Continental crust subduction and ultrahigh pressure metamorphism. *Treatise Geochem.* 3, 293–319. doi:10.1016/b0-08-043751-6/03158-3

Russell, W. A., Papanastassiou, D. A., Tombrello, T. A., Ca isotope fractionation on Salters, V., and Stracke, A. (1978). Composition of the depleted mantle. *Geochem. Geophys. Geosystems*, 5: Q05B07. doi:10.1029/2003GC000597

Salters, V., and Stracke, A. (2004). Composition of the depleted mantle. *Geochem. Geophys. Geosystems* 5, Q05B07. doi:10.1029/2003GC000597

Schmidt, M., and Poli, S. (2003). Generation of mobile components during subduction of oceanic crust. *Treatise Geochem.* 3, 567–591. doi:10.1016/b0-08-043751-6/03034-6

Shi, R., Yang, J., Wu, C., Iizuka, T., and Hirata, T. (2006). Island arc volcanic rocks in the north Qaidam UHP belt, northern Tibet plateau: evidence for ocean-continent subduction preceding continent-continent subduction. *J. Asian Earth Sci.* 28 (2-3), 151–159. doi:10.1016/j.jseaes.2005.09.019

Song, S., Niu, Y., Zhang, G., and Zhang, L. (2019). Two epochs of eclogite metamorphism link 'cold' oceanic subduction and 'hot' continental subduction, the North Qaidam UHP belt, NW China. In: L. Zhang, Z. Zhang, et al.L. Zhang, Z. Zhang, H. Schertl, and C. Wei (Editors), *HP-UHP metamorphism and tectonic evolution of orogenic belts. Geological society, London, special publications*, 474 (1), 275–289. doi:10.1144/sp474.2

Song, S., Niu, Y., Zhang, L., and Zhang, G. (2009a). Time constraints on orogenesis from oceanic subduction to continental subduction, collision, and exhumation: an example from North Qilian and North Qaidam HP-UHP belts. *Acta Petrol. Sin.* 25 (9), 2067–2077.

Song, S., Su, L., Li, X., Zhang, G., Niu, Y., and Zhang, L. (2010). Tracing the 850-Ma continental flood basalts from a piece of subducted continental crust in the North Qaidam UHPM belt, NW China. *Precambrian Res.* 183 (4), 805–816. doi:10.1016/j.precamres.2010.09.008

Song, S., Su, L., Li, X. H., Niu, Y., and Zhang, L. (2012). Grenville-age orogenesis in the qaidam-qilian block: the link between South China and Tarim. *Precambrian Res.* 220, 9–22. doi:10.1016/j.precamres.2012.07.007

Song, S., Su, L., Niu, Y., Zhang, G., and Zhang, L. (2009b). Two types of peridotite in North Qaidam UHPM belt and their tectonic implications for oceanic

and continental subduction: a review. *J. Asian Earth Sci.* 35 (3-4SI), 285–297. doi:10.1016/j.jseaes.2008.11.009

Song, S., Su, L., Niu, Y., Zhang, L., and Zhang, G. (2007). Petrological and geochemical constraints on the origin of garnet peridotite in the North Qaidam ultrahigh-pressure metamorphic belt, northwestern China. *Lithos* 96 (1-2), 243–265. doi:10.1016/j.lithos.2006.09.017

Song, S., Wang, M., Wang, C., and Niu, Y. (2015). Magmatism during continental collision, subduction, exhumation and mountain collapse in collisional orogenic belts and continental net growth: a perspective. *Sci. China Earth Sci.* 58 (8), 1284–1304. doi:10.1007/s11430-015-5102-x

Song, S. G., Niu, Y., Su, L., Zhang, C., and Zhang, L. (2014). Continental orogenesis from ocean subduction, continent collision/subduction, to orogen collapse, and orogen recycling: the example of the North Qaidam UHPM belt, NW China. *Earth-Science Rev.* 129, 59–84. doi:10.1016/j.earscirev.2013.11.010

Song, S. G., Yang, J. S., Liou, J. G., Wu, C., Shi, R., and Xu, Z. (2003a). Petrology, geochemistry, and isotopic ages of eclogites from the dulan UHPM terrane, the North Qaidam, NW China. *Lithos* 70 (3-4), 195–211. doi:10.1016/s0024-4937(03)00099-9

Song, S. G., Yang, J. S., Xu, Z. Q., Liou, J. G., and Shi, R. D. (2003b). Metamorphic evolution of the coesite-bearing ultrahigh-pressure terrane in the North Qaidam, northern tibet, NW China. *J. Metamorph. Geol.* 21 (6), 631–644. doi:10.1046/j.1525-1314.2003.00469.x

Song, S. G., Zhang, L. F., Niu, Y. L., Su, L., Jian, P., and Liu, D. (2005). Geochronology of diamond-bearing zircons from garnet peridotite in the North Qaidam UHPM belt, Northern Tibetan Plateau: a record of complex histories from oceanic lithosphere subduction to continental collision. *Earth Planet. Sci. Lett.* 234 (1-2), 99–118. doi:10.1016/j.epsl.2005.02.036

Song, S. G., Zhang, L. Z. L., Niu, Y. N. Y., Su, L., Song, B., and Liu, D. (2006). Evolution from oceanic subduction to continental collision: a case study from the northern Tibetan plateau based on geochemical and geochronological data. *J. Petrology* 47 (3), 435–455. doi:10.1093/petrology/egi080

Sun, H. S., Li, H., Algeo, T. J., Gabo-Ratio, J. A. S., Yang, H., Wu, J., et al. (2018). Geochronology and geochemistry of volcanic rocks from the tanjianshan group, NW China: implications for the early palaeozoic tectonic evolution of the North Qaidam orogen. *Geol. J.* 54 (3), 1769–1796. doi:10.1002/gj.3268

Sun, Q., Zhao, X., Xue, C., Seltmann, R., McClenaghan, S. H., Chu, H., et al. (2022). Two episodes of Late Paleozoic mafic magmatism in the western Tianshan Orogen: from Carboniferous subduction to Permian post-collisional extension. *Gondwana Res.* 109, 518–535. doi:10.1016/j.gr.2022.06.002

Sun, W., and McDonough, W. (1989). Chemical and isotopic systematics of oceanic basalts: implications for mantle composition and processes. *Earth other Sol. Syst. Mater. Geochimica Cosmochimica Acta* 42 (8): 1075–1090. doi:10.1144/gsl.sp.1989.042.01.19

Villaseca, C., Orejana, D., Higueras, P., Pérez-Soba, C., García Serrano, J., and Lorenzo, S. (2022). The evolution of the subcontinental mantle beneath the Central Iberian Zone: geochemical tracking of its mafic magmatism from the Neoproterozoic to the Cenozoic. *Earth-Science Rev.* 228, 103997. doi:10.1016/j.earscirev.2022.103997

Wang, L., Wang, H., He, C., Chen, N., Santosh, M., Sun, M., et al. (2016). Mesoproterozoic continental breakup in NW China: evidence from gray gneisses from the North Wulan terrane. *Precambrian Res.* 281, 521–536. doi:10.1016/j.precamres.2016.06.016

Wang, M., Song, S., Niu, Y., and Su, L. (2014). Post-collisional magmatism: consequences of UHPM terrane exhumation and orogen collapse, N. Qaidam UHPM belt, NW China. *Lithos* 210, 181–198. doi:10.1016/j.lithos.2014.10.006

Wang, Q., Dong, Y., Pan, Y., Liao, F., and Guo, X. (2018). Early paleozoic granulite-facies metamorphism and magmatism in the northern wulan terrane of the quanji massif: implications for the evolution of the proto-tethys ocean in northwestern China. *J. Earth Sci.* 29, 1081–1101. doi:10.1007/s12583-018-0881-6

Willbold, M., and Stracke, A. (2010). Formation of enriched mantle components by recycling of upper and lower continental crust. *Chem. Geol.* 276 (3), 188–197. doi:10.1016/j.chemgeo.2010.06.005

Winchester, J. A., and Floyd, P. A. (1977). Geochemical discrimination of different magma series and their differentiation products using immobile elements. *Chem. Geol.* 20, 325–343. doi:10.1016/0009-2541(77)90057-2

Wood, D. A. (1980). The application of a Th, Hf, Ta diagram to problems of tectono-magmatic classification and to establishing the nature of crustal contamination of basaltic lavas of the British Tertiary Volcanic Province. *Earth Planet. Sci. Lett.* 50 (1), 11–30. doi:10.1016/0012-821x(80)90116-8

Workman, R. K., and Hart, S. R. (2005). Major and trace element composition of the depleted MORB mantle (DMM). *Earth Planet. Sci. Lett.* 231 (1), 53–72. doi:10.1016/j.epsl.2004.12.005

Workman, R. K., Hart, S. R., Blusztajn, J., Jackson, M., Kurz, M., and Staudigel, H. (2003). "Enriched mantle II: a new view from the Samoan hotspot," in *EGS-AGU-EUG joint assembly*.13656

Wu, C., Gao, Y., Li, Z., Lei, M., Qin, H., Li, M., et al. (2014). Zircon SHRIMP U-Pb dating of granites from Dulan and the chronological framework of the North Qaidam UHP belt, NW China. *Sci. China Earth Sci.* 57 (12), 2945–2965. doi:10.1007/s11430-014-4958-5

Wu, C., Yuanhong, G., Suoping, W., QiLong, C., Wooden, J. L., Mazadab, F. K., et al. (2007). Zircon SHRIMP U-Pb dating of granites from the Da Qaidam area in the north margin of Qaidam basin, NW China. *Acta Petrol. Sin.* 23 (8), 1861–1875.

Wu, C., Wu, D., Mattinson, C., Lei, M., and Chen, H. (2019). Petrogenesis of granitoids in the Wulan area: magmatic activity and tectonic evolution in the North Qaidam, NW China. *Gondwana Res.* 67, 147–171. doi:10.1016/j.gr.2018.09.010

Wu, T., Xiao, L., Ma, C., Pirajno, F., Sun, Y., and Zhan, Q. (2014). A mafic intrusion of "arc affinity" in a post-orogenic extensional setting: a case study from Ganluogou gabbro in the northern Yidun Arc Belt, eastern Tibetan Plateau. *J. Asian Earth Sci.* 94, 139–156. doi:10.1016/j.jseaes.2014.08.026

Wu, Y., and Zheng, Y. (2004). Genesis of zircon and its constraints on interpretation of U-Pb age. *Chin. Sci. Bull.* 49 (15), 1554–1569. doi:10.1360/04wd0130

Xiong, Q., Griffin, W. L., Zheng, J., O Reilly, S. Y., and Pearson, N. J. (2015). Episodic refertilization and metasomatism of Archean mantle: evidence from an orogenic peridotite in North Qaidam (NE Tibet, China). *Contributions Mineralogy Petrology* 169 (3), 31. doi:10.1007/s00410-015-1126-7

Xiong, Q., Zheng, J., Griffin, W. L., O' Reilly, S. Y., and Pearson, N. J. (2014). Pyroxenite dykes in orogenic peridotite from North Qaidam (NE tibet, China) track metasomatism and segregation in the mantle wedge. *J. Petrology* 55 (12), 2347–2376. doi:10.1093/petrology/egu059

Xiong, Q., Zheng, J., Griffin, W. L., O'Reilly, S. Y., and Zhao, J. (2011). Zircons in the Shenglikou ultrahigh-pressure garnet peridotite massif and its country rocks from the North Qaidam terrane (western China): meso-Neoproterozoic crust-mantle coupling and early Paleozoic convergent plate-margin processes. *Precambrian Res.* 187 (1-2), 33–57. doi:10.1016/j.precamres.2011.02.003

Yang, J., Shi, R., Wu, C., and Chen, S. (2004). Recognition of Neoproterozoic ophiolite on the northern margin of the Qaidam basin: evidence of the breakup of Rodinia? *Geol. Bull. China* (Z2), 892–898.

Yang, J., Wu, C., Zhang, J., Shi, R., Meng, F., Wooden, J., et al. (2006). Protolith of eclogites in the north Qaidam and Altun UHP terrane, NW China: earlier oceanic crust? *J. Asian Earth Sci.* 28 (2-3), 185–204. doi:10.1016/j.jseaes.2005.09.020

Yang, J., Xu, Z., Song, S., Zhang, J., Wu, C., Shi, R., et al. (2001). Discovery of coesite in the North Qaidam Early Palaeozoic ultrahigh pressure (UHP) metamorphic belt, NW China. *Comptes Rendus de l'Académie des Sci. - Ser. IIA - Earth Planet. Sci.* 333 (11), 719–724. doi:10.1016/s1251-8050(01)01718-9

Yu, S., Zhang, J., Li, H., Hou, K., Mattinson, C., and Gong, J. (2013). Geochemistry, zircon U-Pb geochronology and Lu-Hf isotopic composition of eclogites and their host gneisses in the dulan area, North Qaidam UHP terrane: new evidence for deep continental subduction. *Gondwana Res.* 23 (3), 901–919. doi:10.1016/j.gr.2012.07.018

Yu, S. Y., Li, S. Z., Zhang, J. X., Peng, Y., Somerville, I., Liu, Y., et al. (2019). Multistage anatexis during tectonic evolution from oceanic subduction to continental collision: a review of the North Qaidam UHP Belt, NW China. *Earth- Sci. Rev.* 191, 190–211. doi:10.1016/j.earscirev.2019.02.016

Zhang, C., Bader, T., Zhang, L., and van Roermund, H. (2017). The multi-stage tectonic evolution of the Xitieshan terrane, North Qaidam orogen, western China: from Grenville-age orogeny to early-Paleozoic ultrahigh-pressure metamorphism. *Gondwana Res.* 41, 290–300. doi:10.1016/j.gr.2015.04.011

Zhang, C., Zhang, L., Van Roermund, H., Song, S., and Zhang, G. (2011). Petrology and SHRIMP U-Pb dating of Xitieshan eclogite, North Qaidam UHP metamorphic belt, NW China. *J. Asian Earth Sci.* 42 (4SI), 752–767. doi:10.1016/j.jseaes.2011.04.002

Zhang, G., Ellis, D. J., Christy, A. G., Zhang, L., Niu, Y., and Song, S. (2009a). UHP metamorphic evolution of coesite-bearing eclogite from the Yuka terrane, North Qaidam UHPM belt, NW China. *Eur. J. Mineralogy* 21 (6), 1287–1300. doi:10.1127/0935-1221/2009/0021-1989

Zhang, G., Zhang, L., and Christy, A. G. (2013). From oceanic subduction to continental collision: an overview of HP-UHP metamorphic rocks in the North Qaidam UHP belt, NW China. *J. Asian Earth Sci.* 63 (SI), 98–111. doi:10.1016/j.jseaes.2012.07.014

Zhang, G. B., Ireland, T., Zhang, L., Gao, Z., and Song, S. (2016). Zircon geochemistry of two contrasting types of eclogite: implications for the tectonic evolution of the North Qaidam UHPM belt, northern Tibet. *Gondwana Res.* 35, 27–39. doi:10.1016/j.gr.2016.04.002

Zhang, G. B., Song, S., Zhang, L., and Niu, Y. (2008). The subducted oceanic crust within continental-type UHP metamorphic belt in the North Qaidam, NW China: evidence from petrology, geochemistry, and geochronology. *Lithos* 104 (1-4), 99–118. doi:10.1016/j.lithos.2007.12.001

Zhang, J., Mattinson, C. G., Meng, F., Yang, H., and Wan, Y. (2009b). U-Pb geochronology of paragneisses and metabasite in the Xitieshan area, north Qaidam Mountains, western China: constraints on the exhumation of HP/UHP metamorphic rocks. *J. Asian Earth Sci.* 35 (3-4SI), 245–258. doi:10.1016/j.jseaes.2008.08.008

Zhang, J., Mattinson, C. G., Meng Fancong, M. F., Wan Yusheng, W. Y., and Tung, K. (2008). Polyphase tectonothermal history recorded in granulitized gneisses from the north Qaidam HP/UHP metamorphic terrane, western China; evidence from zircon U-Pb geochronology. *Geol. Soc. Am. Bull.* 120 (5-6), 732–749. doi:10.1130/b26093.1

Zhang, J., Meng, F., Li, J., and Mattinson, C. G. (2009c). Coesite in eclogite from the North Qaidam mountains and its implications. *Chin. Sci. Bull.* 54 (6), 1105–1110. doi:10.1007/s11434-009-0074-x

Zhang, L., Chen, R., Zheng, Y., Hu, Z., and Xu, L. (2017). Whole-rock and zircon geochemical distinction between oceanic- and continental-type eclogites in the North Qaidam orogen, northern Tibet. *Gondwana Res.* 44, 67–88. doi:10.1016/j.gr.2016.10.021

Zhang, L., Chen, R., Zheng, Y., Li, W. C., Hu, Z., Yang, Y., et al. (2016). The tectonic transition from oceanic subduction to continental subduction: zirconological constraints from two types of eclogites in the North Qaidam orogen, northern Tibet. *Lithos* 244, 122–139. doi:10.1016/j.lithos.2015.12.003

Zhang, L., Chen, R. X., Zheng, Y. F., and Hu, Z. (2015). Partial melting of deeply subducted continental crust during exhumation: insights from felsic veins and host UHP metamorphic rocks in North Qaidam, northern Tibet. *J. Metamorph. Geol.* 33, 671–694. doi:10.1111/jmg.12146

Zhang, L., Lü, Z., Zhang, G., and Song, S. (2008). The geological characteristics of oceanic-type UHP metamorphic belts and their tectonic implications: case studies from Southwest Tianshan and North Qaidam in NW China. *Sci. Bull.* 53 (20), 3120–3130. doi:10.1007/s11434-008-0386-2

Zhao, J., and Zhou, M. (2007). Geochemistry of Neoproterozoic mafic intrusions in the Panzhihua district (Sichuan Province, SW China): implications for subduction-related metasomatism in the upper mantle. *Precambrian Res.* 152 (1), 27–47. doi:10.1016/j.precamres.2006.09.002

Zhao, Z., Dai, L., and Zheng, Y. (2013). Postcollisional mafic igneous rocks record crust-mantle interaction during continental deep subduction. *Sci. Rep.* 3 (1), 3413. doi:10.1038/srep03413

Zhao, Z., Dai, L., and Zheng, Y. (2015). Two types of the crust-mantle interaction in continental subduction zones. *Sci. China Earth Sci.* 58, 1269–1283. doi:10.1007/s11430-015-5136-0

Zhao, Z., Wei, J., Fu, L., Liang, S., and Zhao, S. (2017). The Early Paleozoic Xitieshan syn-collisional granite in the North Qaidam ultrahigh-pressure metamorphic belt, NW China: petrogenesis and implications for continental crust growth. *Lithos* 278-281, 140–152. doi:10.1016/j.lithos.2017.01.019

Zhao, Z., Wei, J., Santosh, M., Liang, S., Fu, L., Zhao, S., et al. (2018). Late Devonian post-collisional magmatism in the ultrahigh-pressure metamorphic belt, Xitieshan terrane, NW China. *Geol. Soc. Am. Bull.* 130 (5-6), 999–1016. doi:10.1130/b31772.1

Zheng, F., Dai, L., Zhao, Z., Zheng, Y., and Xu, Z. (2019). Recycling of Paleo-oceanic crust: geochemical evidence from Early Paleozoic mafic igneous rocks in the Tongbai orogen, Central China. *Lithos* 328-329, 312–327. doi:10.1016/j.lithos.2019.01.010

Zheng, Y. (2009). Fluid regime in continental subduction zones: petrological insights from ultrahigh-pressure metamorphic rocks. *J. Geol. Soc.* 166 (4), 763–782. doi:10.1144/0016-76492008-016r

Zheng, Y. (2012). Metamorphic chemical geodynamics in continental subduction zones. *Chem. Geol.* 328, 5–48. doi:10.1016/j.chemgeo.2012.02.005

Zheng, Y. (2019). Subduction zone geochemistry. *Geosci. Front.* 10 (4), 1223–1254. doi:10.1016/j.gsf.2019.02.003

Zheng, Y., and Chen, R. (2017). Regional metamorphism at extreme conditions: implications for orogeny at convergent plate margins. *J. Asian Earth Sci.* 145, 46–73. doi:10.1016/j.jseaes.2017.03.009

Zheng, Y., and Hermann, J. (2014). Geochemistry of continental subduction-zone fluids. *Earth, planets, space* 66 (1), 93–16. doi:10.1186/1880-5981-66-93

Zheng, Y., Xia, Q., Chen, R., and Gao, X. (2011). Partial melting, fluid supercriticality and element mobility in ultrahigh-pressure metamorphic rocks during continental collision. *Earth-Science Rev.* 107 (3), 342–374. doi:10.1016/j.earscirev.2011.04.004

Zheng, Y., Xu, Z., Zhao, Z., and Dai, L. (2018). Mesozoic mafic magmatism in North China: implications for thinning and destruction of cratonic lithosphere. *Sci. China Earth Sci.* 61, 353–385. doi:10.1007/s11430-017-9160-3

Zheng, Y., Zhao, Z., and Chen, R. (2019). Ultrahigh-pressure metamorphic rocks in the Dabie-Sulu orogenic belt: compositional inheritance and metamorphic modification. *Geol. Soc. Lond. Spec. Publ.* 474 (1), 89–132. doi:10.1144/sp474.9

Zhou, C. A., Song, S., Allen, M. B., Wang, C., Su, L., and Wang, M. (2021). Post-collisional mafic magmatism: insights into orogenic collapse and mantle modification from North Qaidam collisional belt, NW China. *Lithos* 398, 106311. doi:10.1016/j.lithos.2021.106311

Zhou, G., Zhang, J., Yu, S., Li, Y., Lu, Z., Mao, X., et al. (2019). Metamorphic evolution of eclogites and associated metapelites from the Yuka terrane in the North Qaidam ultrahigh pressure metamorphic belt, NW China: constraints from phase equilibrium modeling. *J. Asian Earth Sci.* 173, 161–175. doi:10.1016/j.jseaes.2019.01.017

Zhu, X., Chen, D., Liu, L., Zhao, J., and Zhang, L. (2014). Geochronology, geochemistry, and significance of the Early Paleozoic back-arc type ophiolite in Luliangshan area, North Qaidam. *Acta Petrol. Sin.* 30 (3), 822–834.

Zhu, X., Chen, D., Wang, C., Wang, H., and Liu, L. (2015). The initiation, development and termination of the neoproterozoic-early Paleozoic ocean in the northern margin of Qaidam basin. *Acta Geol. Sin.* 89 (02), 234–251.

Zhu, X. H., Chen, D. L., Liu, L., and Li, D. (2010). Zircon LA-ICP-MS U-Pb dating of the Wanggaxiu gabbro complex in the Dulan area, northern margin of Qaidam Basin, China and its geological significance. *Geol. Bull. China* 29, 227–236.

Zhu, X. H., Chen, D. L., Liu, L., Wang, C., Yang, W. Q., Cao, Y. T., et al. (2012). Chronology and geochemistry of the mafic rocks in Xitieshan area, North Qaidam. *Geol. Bull. China* 31 (12), 2079–2089.

Zindler, A., and Hart, S. (1986). Chemical geodynamics. *Annu. Rev. Earth Planet. Sci.* 14 (1), 493–571. doi:10.1146/annurev.earth.14.1.493

Zong, K., Klemd, R., Yuan, Y., He, Z., Guo, J., Shi, X., et al. (2017). The assembly of Rodinia: the correlation of early Neoproterozoic (ca. 900Ma) high-grade metamorphism and continental arc formation in the southern Beishan Orogen, southern Central Asian Orogenic Belt (CAOB). *Precambrian Res.* 290, 32–48. doi:10.1016/j.precamres.2016.12.010

Zou, H., Zindler, A., Xu, X., and Qi, Q. (2000). Major, trace element, and Nd, Sr and Pb isotope studies of Cenozoic basalts in SE China: mantle sources, regional variations, and tectonic significance. *Chem. Geol.* 171 (1), 33–47. doi:10.1016/s0009-2541(00)00243-6